Report 13, 1990

THE GRAVITY STRUCTURE OF EBURRU, KENYA

Silas Masinde Simiyu,
UNU Geothermal Training Programme,
Orkustofnun - National Energy Authority,
Grensasvegur 9,
108 Reykjavik,
ICELAND

Permanent address:
KPC Geothermal,
Box 785,
Naivasha,
KENYA

ABSTRACT

Gravity data show that the Eburru area has a complex gravity structure. The results show a N-S axial high along a graben caused by dense intrusives along N-S fault zones and at major structural intersections within the area. Low frequency filtering delineates a major NE-SW negative anomaly modelled as a basin structure, at whose intersection with the N-S graben occurs the Eburru caldera. Within it, one well has been drilled with a 2.5 MWe production capacity. High frequency anomalies are related to vertical intrusives at shallow depths, occurring at fault junctions. Analysis of these anomalies has led to a proper definition of a NW-SE structural and resistivity discontinuity, dividing the study area into two regions. This has also led to the confinement of the Eburru caldera boundaries. Fluid feed for the geothermal system is along vertical conduits and the heat coming from narrow intrusive bodies at fault junctions.

TABLE OF CONTENTS

LIST OF FIGURES

Page

1. INTRODUCTION

1.1 Aim of the project

During the Eburru scientific review meeting of 1986, it was recommended that a detailed gravity survey be undertaken in the prospect area. This was to add to 101 UNDP and 40 Leicester University gravity stations which were unevenly and widely spread.

In the present study, the writer uses gravity data from 732 stations he surveyed between 1988 and 1990, and the UNDP and Leicester University gravity data to determine the Eburru gravity structure. The interpretation aim is to schematize the major Eburru gravity structural trends without exact details which may need more accurate control from detailed seismic and geological data.

1.2 Location

The Eburru geothermal prospect lies about 30 km north of the Olkaria geothermal field (Figure 1). Both geothermal areas occur within the eastern arm of the East African Rift valley. The Eburru prospect area under consideration extends from UTM grid reference east 182000 to 210000 and north 9914000 to 9950000. The presumed centre of the prospect is located near the Eburru crater, which has an elevation of about 2,700 m above sea level.

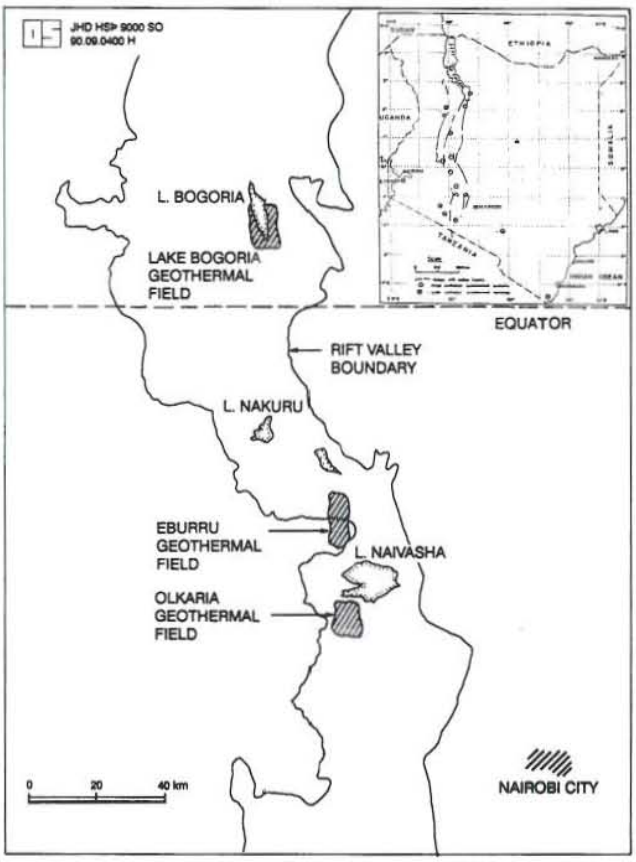

FIGURE 1: Locality map of Eburru geothermal field in the Rift valley

1.3 Previous work

Much work had been done around the Naivasha area by private individuals in the latter part of the 20th century. Systematic geological mapping was conducted between 1955 and 1956 by Thomson and Dodson (1963) in view of the geothermal power potential of the area. Since then, other groups have engaged in more thorough work on geothermal energy exploration. A detailed integrated exploration study of the Eburru geothermal prospect began in 1972 as a joint project of the UNDP and the Kenya Government. This involved geological mapping, geochemical sampling of fumeroles and a regional gravimetric survey. JICA, in cooperation with the Ministry of Energy, did more work in 1983. In 1986, KPC geophysical staff extended the resistivity survey. A detailed aeromagnetic survey was flown by Geosurvey International the same year (Figure 2).

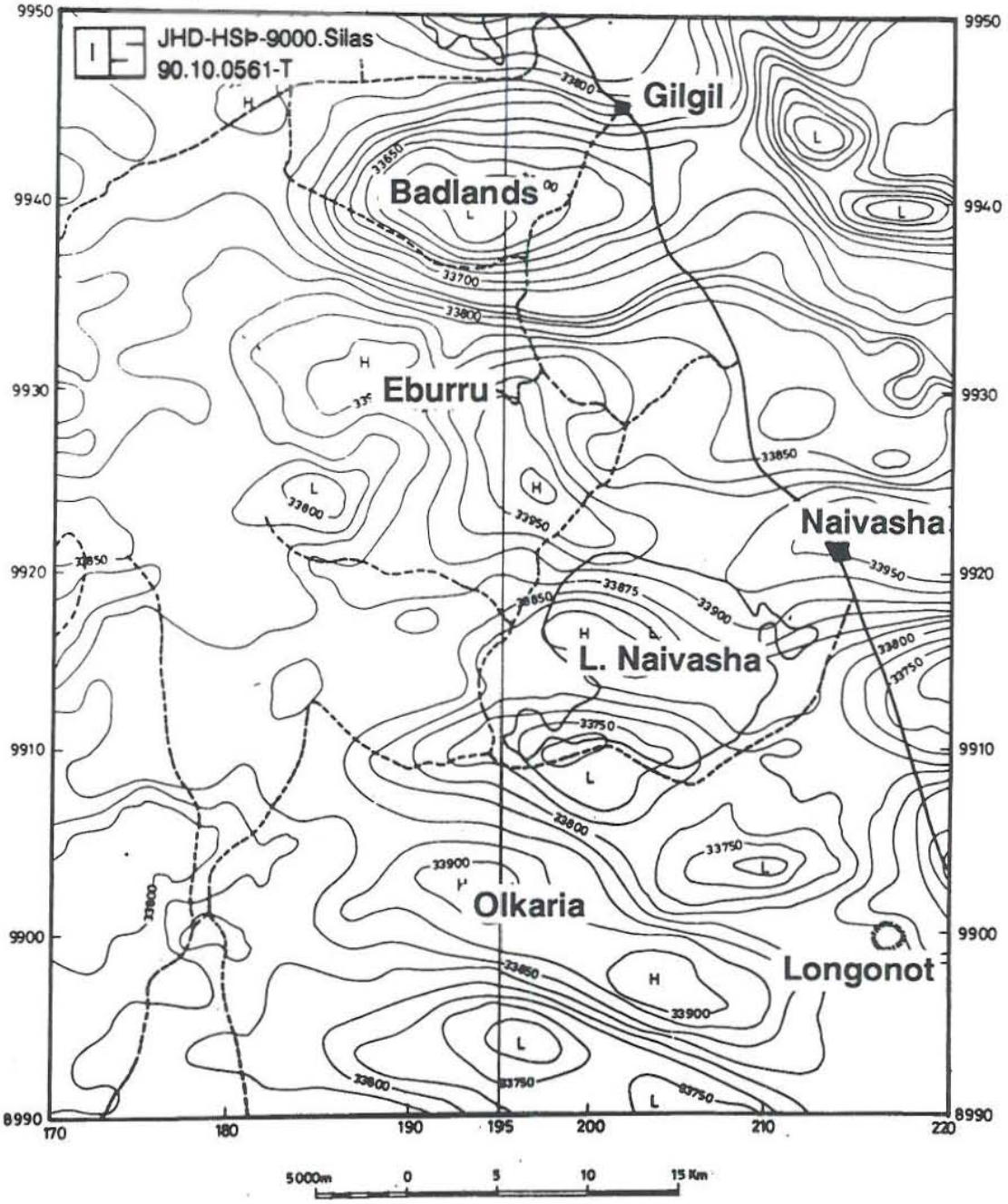

FIGURE 2: Total magnetic field anomaly map of Eburru

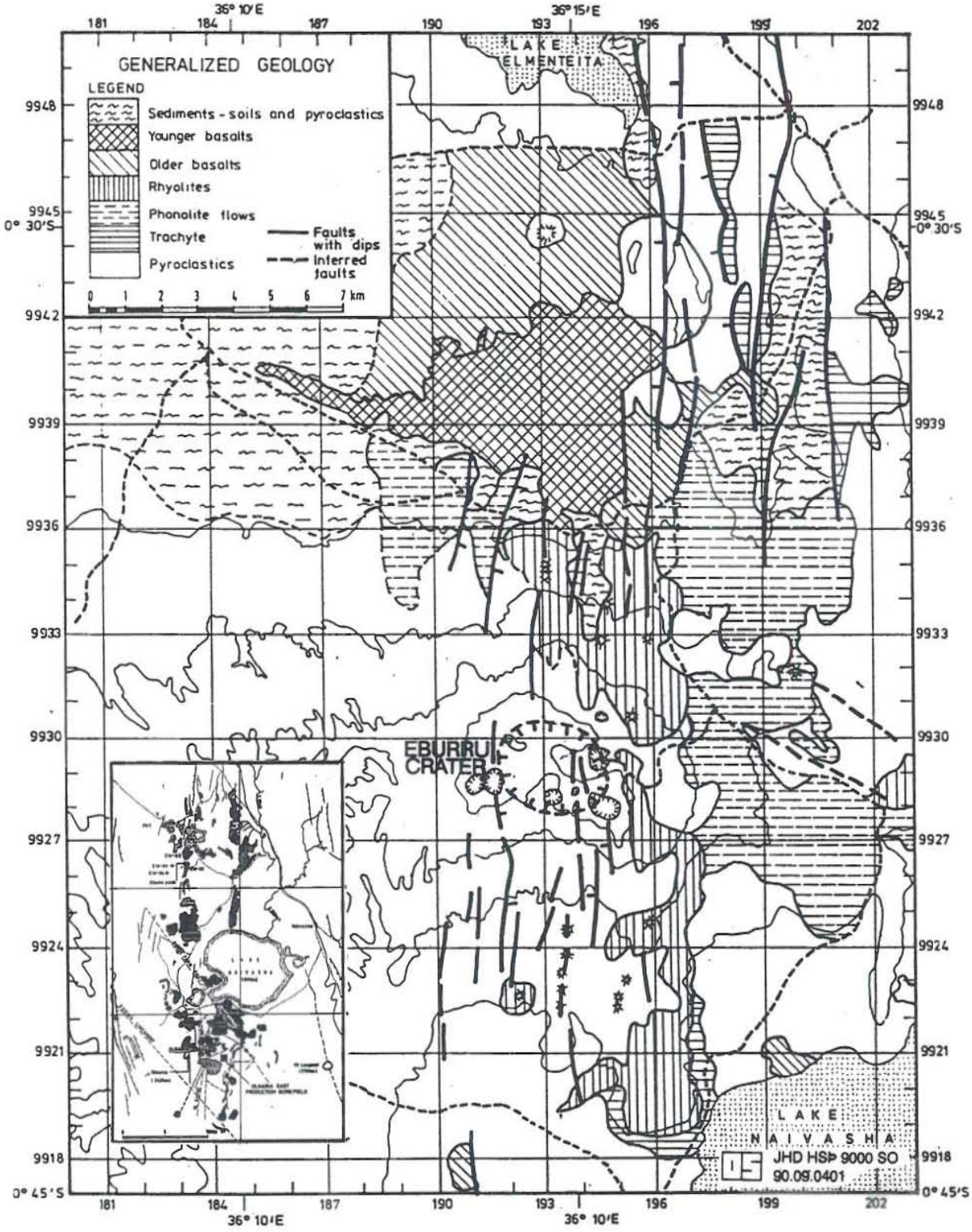

FIGURE 3: Simplified geology of the Eburru area

The aeromagnetic data show a WNW-ESE ridge of high magnetic field strength extending from Eburru mountain to lake Naivasha, and an area of very low field strength correlating with the Badlands basalts. The WNW-ESE anomaly was interpreted by KPC (1986) as being caused by

demagnetization, and the low magnetic field strength anomaly around the Badlands was interpreted as being due to the basalts having been emplaced during the present magnetic epoch, as such, having high magnetic susceptibility.

Recent modelling by a University of Auckland student (Ng'ang'a, 1989) shows that the magnitude of the Badlands basalt anomaly can only be explained by a deep body, probably the source of the surface basalts. Due to time constraints, the modelling was never completed. The UNDP and Leicester University gravity data had restricted coverage and did not show any anomalies of interest. A Bouguer density of 2.67×10^{3} kgm^{-3} was used to reduce the data and this caused a negative anomaly over Eburru hill, which meant that the density value used was too high. No regional anomaly was removed and, therefore, the residual anomaly interpretation cannot be reliable.

During the Eburru scientific review meeting of 1986 (KPC, 1986), resistivity data was heavily relied upon to propose the location of the first four wells drilled, because gravity and magnetics did not yield any useful information.

1.4 Geology

Pyroclastic deposits are widespread around the Eburru prospect. These rocks occur in the western part of the Eburru crater covering the Eburru forest area. The eastern and southern parts are covered by young deposits which can also be found scattered in the north. The type of rocks identified in the area include comendites, phonolites, obsidians, trachytes, rhyolites and basalts of upper Pleistocene (Figure 3). The Badlands basalts in the north are of recent age and are not covered by vegetation. The flows to the south are mainly rhyolites, comendites, trachytes and minor basalts.

The structures found in the area include caldera-like features and numerous N-S faults (Figure 3). Two categories of faults are recognisable, including older rift faults and young faults on the rift floor. The older rift faults trend in a NW-SE direction. For both categories of faults, those to the west are downthrown to the east while those to the east are downthrown to the west, hence forming a graben structure.

The Eburru area is located within the Rift valley at a point where the valley shifts from a north-south trend to a more northwesterly trend (Figure 1). This might be of significance in view of the rift faults meeting at an angle in this place and frictional resistance to opening up, thus making Eburru the narrowest part of the Rift valley.

Young faults cut through the Eburru hill and trend N-S. In some parts, they appear as open fissures. The craters and lava flows appear to occur along faults and fault junctions. All the faults occur as normal faults along which most of the geothermal manifestations are confined. The main Eburru crater lies within a young N-S trending fault zone containing numerous vertical faults. The faults within the crater are covered by volcanic ash and pyroclastics but are associated with smaller collapse craters and aligned fumeroles and hot ground. Where they cut the inside walls of the crater, numerous fumeroles are evident. These faults allow the ascent of vapour and probably provide permeable channels at depth. The main Eburru volcanic centre is composed of numerous volcanic craters, some of which suggest a ring structure.

2. GRAVITY MEASUREMENTS

Gravity measurements were made using a Lacoste and Romberg gravity meter in closed loops. Each loop was tied to the nearest of 8 base stations carefully located to ensure adequate coverage (Figure 4). Drift and tidal corrections were done to all stations on a daily basis. The measurements were then reduced to a primary base station (Base 1, Figure 4). The primary Base 1 station is located at Eburru primary school, UTM grid reference (195600E, 9928800N), gravity value 9773263.7 g.u. (gravity unit = 10^{-6} ms^{-2}). This value was referred to as the Safariland base station number A2 value 977460.75 g.u., established by Geothermica Italiana, who tied this station to the Nairobi International Base station IGSN71 having a value of 9775260.70 g.u.

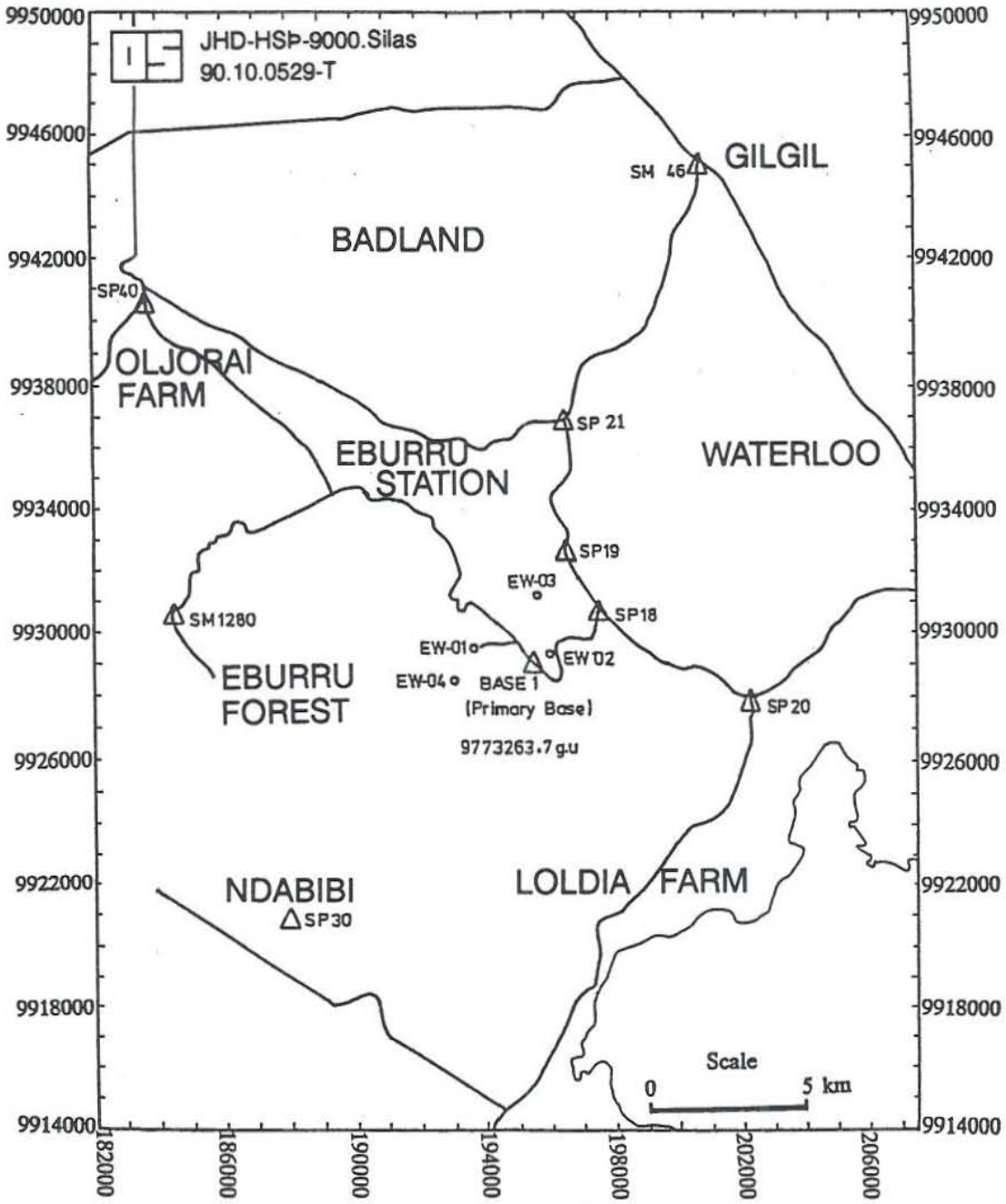

FIGURE 4: Gravity base stations' location map

3. DATA REDUCTION

3.1 Gravity formula

The theoretical sea-level gravity, δ, at latitude Φ in degrees, has been calculated from the 1967 gravity formula (Swain and Khan, 1977). This is approximated as:

$$\delta = 9{,}780{,}318.5 \text{ X } (1+0.005{,}278{,}895 \sin^2\Phi + 0.000{,}023{,}462 \sin^4\Phi) \text{ g.u.},$$

which is accurate to 0.04 g.u.

3.2 Free air anomaly

The free air anomalies (F.A.A.) were calculated by continuing upward the sea level theoretical gravity to the station height, using the free air correction factor and subtracting this from the observed gravity. Thus:

$$\text{F.A.A.} = g_o-(\delta-3.086h) \text{ g.u.}, \quad \text{where h = height in m.}$$

3.3 Simple Bouguer anomaly

The Bouguer and terrain corrections depend on the density of subsurface material within the range of station elevation differences. The density value used for both Bouguer and terrain corrections was determined first.

The simple Bouguer anomaly (S.B.A.) was calculated by subtracting from the free air anomaly the effect of an infinite slab of thickness equal to the station height h and density σ, using;

$$\text{S.B.A.} = \text{F.A.A.} - 2\pi G\sigma h,$$

where G = the gravitational constant = $6.67\text{x}10^{-11}$ $m^3kg^{-1}s^{-2}$.

3.4 Terrain corrections

The terrain corrections were made using Hammer charts for the B C D and E zones on maps of scale 1:10,000. For the outer zone, a digitized topography was used to compute the terrain corrections using a computer program.

The terrain in and around the survey area was digitized into two grids with data spacings of 500 m and 1,500 m. The 500 m grid was interpolated using a cubic spline to 100 m spaced points to complete the terrain in a block 2,400 m square, centred on each station. The 1,500 m grid was used to complete terrain corrections from the 2,400 m block to a 24 km square around the station. A 2,500 m grid was used to calculate terrain corrections over a 100 km square block. The exact formula for calculation of a block was used in the inner zone, and line mass approximations for the outer 2 zones. In the outermost zone, correction was also made for the curvature of the earth after the method described by Swain and Khan (1977).

3.5 Complete Bouguer anomaly

The complete Bouguer anomaly (C.B.A.) was calculated using the method of Swain and Khan (1977).

$$C.B.A. = S.B.A. + terrain - B,$$

where B is the correction for the earth curvature effect on a Bouguer plate given as:

$$B = 0.013h - 3.5 \times 10^{-6}h^2 \text{ g.u. (h in m).}$$

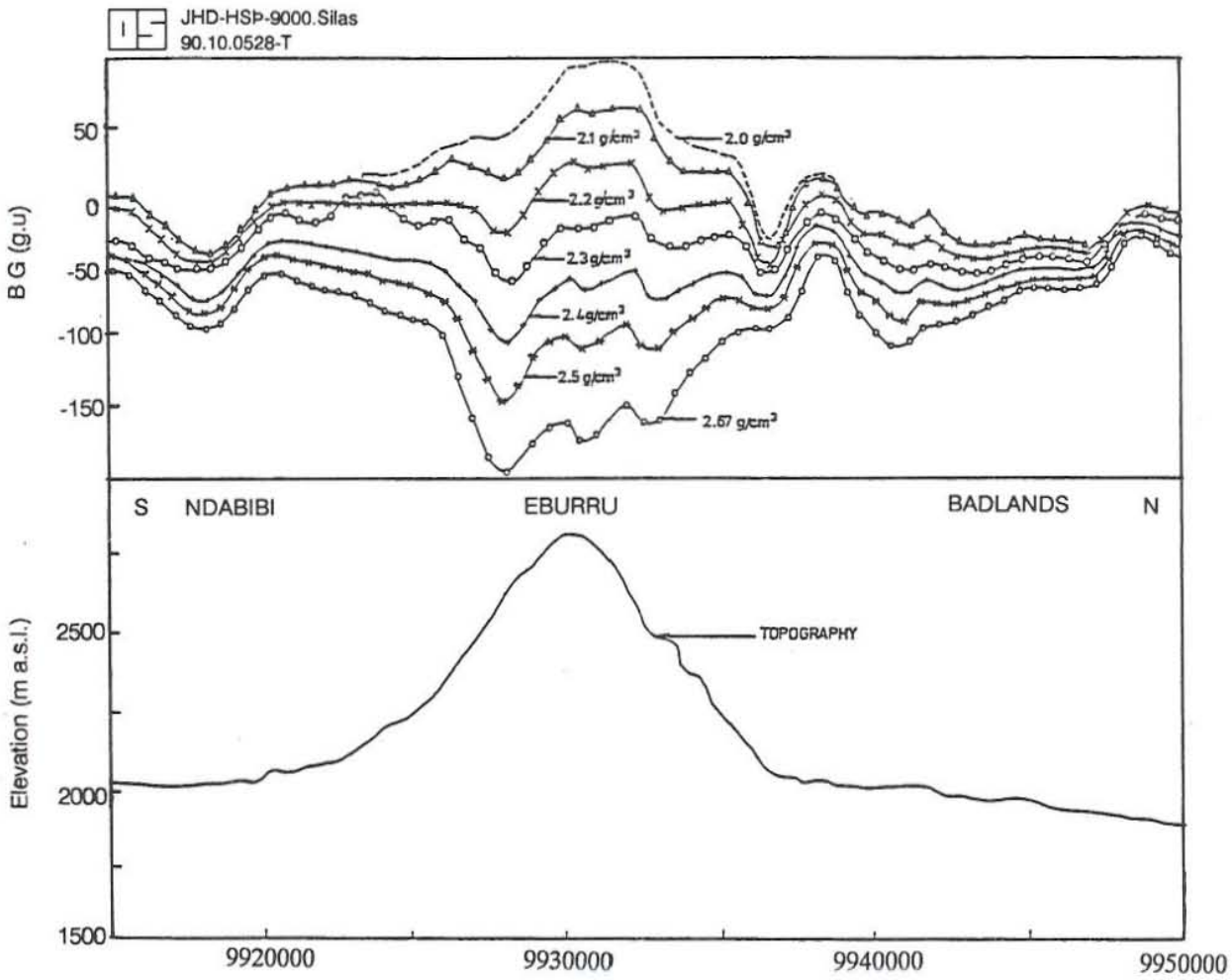

FIGURE 5: Nettleton's Bouguer density determination profiles

4. DENSITY DETERMINATION

4.1 Introduction

The Bouguer and terrain corrections made as part of the reduction of gravity data require knowledge of the average density of the rocks from the surface to the reference spheroid and generally within the topographic differences of the surveyed area. A major difficulty with the gravity method is that there is not yet any satisfactory way to measure the density of rocks in situ.

Topographic features are not geologically homogeneous in the present study area and it is therefore hard to determine a representative density for the whole area. There are such local variations in lithology that determination of an average density is done with a lot of caution.

The available mathematical techniques are tested and their results compared with the known geology to make a decision on the appropriate average density.

4.2 Nettleton's method

This is an indirect density determination method by which one tries to correlate either statistically or visually the relationship between gravity and elevation (Nettleton, 1976). The aim is to get a density value that gives minimum correlation between calculated gravity and elevation. This is based on the assumption that topographic differences in the area are not associated with lithological changes. Different approaches to the method are used.

Profile method. A traverse is made across a topographic feature which is assumed to be lithologically similar to the surrounding rocks. N-S profiles of observed gravity values across Eburru hill were plotted and reductions made at every station. The calculation was repeated a number of times, different densities being assumed for each computation. The resulting profiles, using different densities, were then compared with the topography of the Eburru hill.

Using this method, Figure 5 shows that a density of $2.3x10^3$ kgm^{-3} to $2.4x10^3$ kgm^{-3} gives the least topographically-related profile, and the average density could be within or close to that range.

One disadvantage with this method is that it gives correct densities only at shallow horizons, that is within the elevation differences of the survey and may, therefore, tend to give densities lower than the true ones.

The gravity-elevation plot method is similar to the profile method except that here the station gravity values at different densities are plotted against elevation and then a best fit line is drawn through the points and checked for gravity dependence on elevation. The density that gives a fit with the least dependence is taken to be the approximate density.

After making plots for density values ranging from $2.0x10^3$ kgm^{-3} to $2.7x10^3$ kgm^{-3} (Figure 6), they show that the area's density can be divided into three broad zones. Rocks of high densities above $2.6x10^3$ kgm^{-3} below 2,200 m a.s.l., rocks of density ranging from $2.5x10^3$ kgm^{-3} to $2.4x10^3$ kgm^{-3} from 2,200 to 2,400 m a.s.l. and less than $2.3x10^3$ kgm^{-3} above this level. The density values obtained from these plots are supported by the known geology of pyroclastics with volcanic ash at high elevations and trachytes with basalts at lower elevations.

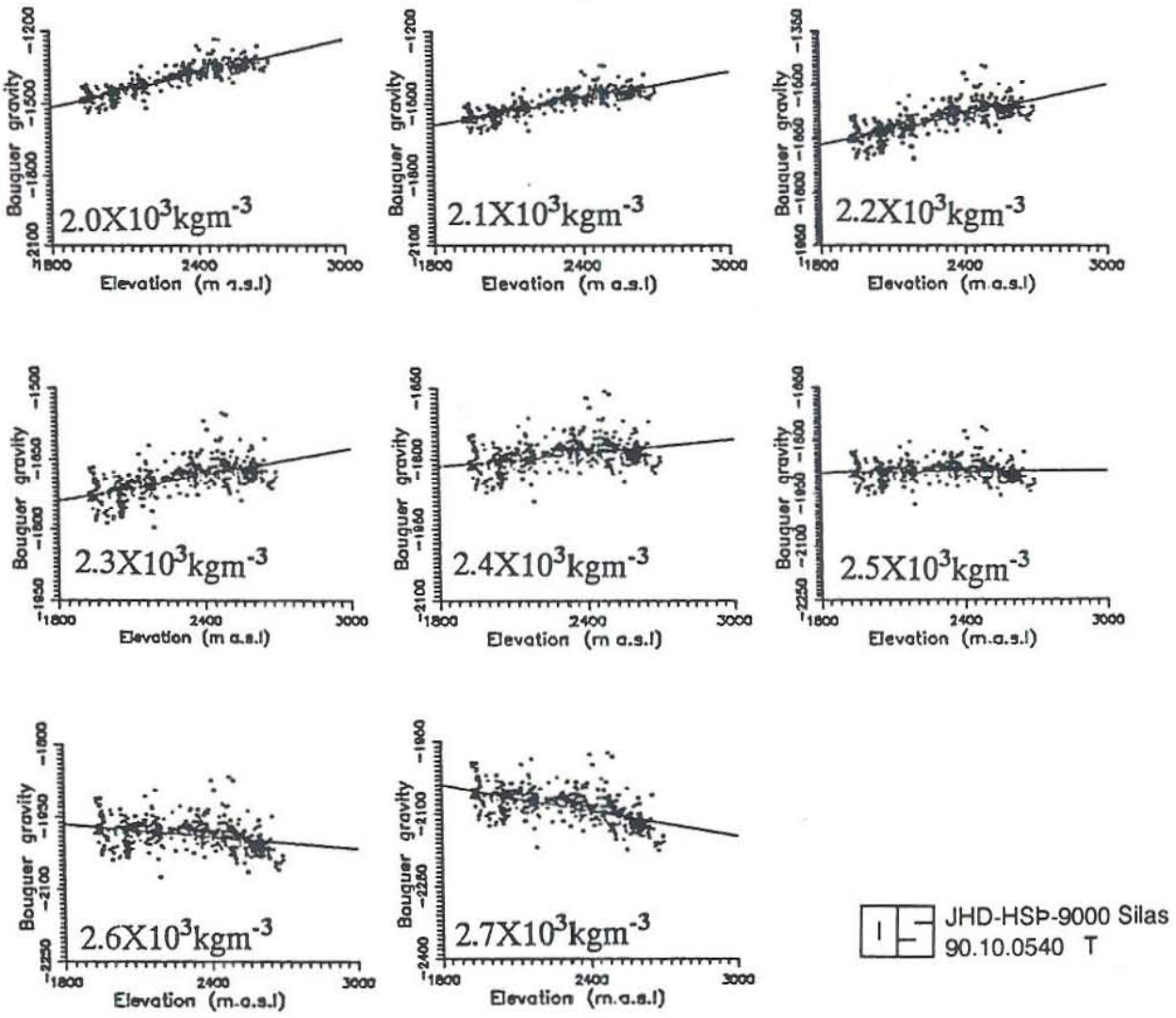

FIGURE 6: Bouguer gravity vs elevation plots

To determine an average density, the $2.5x10^3$ kgm^{-3} scatter had the least gravity-elevation correlation with a near-zero slope best fit line and is, therefore, taken to be the best density for this method. When the data and elevation correlation was done using a program that outputs the coefficient of correlation at different densities, a density of $2.49x10^3$ kgm^{-3} gave a zero correlation coefficiency.

4.3 Fractal analysis method

Fractal analysis of the data was carried out by using the method described by Thorarinsson and Magnusson (1990). A ten kilometre circularly windowed data within the area of nearly uniform and highest density of data coverage is used. First the analysis was applied on the elevation data and a 7 km range was found to be fractal. The analysis of different density data followed

with the fractal dimensions being determined over the 7 km range. This method gave a density of $2.3x10^3$ kgm^{-3} as the best value for the area. This method could have been limited by the uneven spread of data and the choosing of the data used from a higher elevation area where the spread was better and, therefore, lowered the overall density.

4.4 Direct measurement on drill cores

Drill core measurements show a density of less than $2.4x10^3$ kgm^{-3} above 2,000 m a.s.l. (Figure 7). Below this level, the average density is about $2.5x10^3$ kgm^{-3} becoming higher as the elevation decreases. Over a longer interval of depth the densities appear to follow a trend. If we assume a smooth best fit curve through the points, we find that there is a general increase of density with depth which is a true formational density. If a horizontal linear best fit line is assumed, an average density of about $2.45x10^3$ kgm^{-3} is determined.

During density measurements on drilled cores or rock samples, there is always a tendency to use nicely consolidated cores which are easy to cut into regular shapes. This leads to the determined densities being higher than the actual rock bulk density.

4.5 Conclusions

The analytical and geological information show that the area does not have uniform density rocks. The density varies from about $2.2x10^3$ kgm^{-3} at high elevations such as Eburru hill to values more than $2.6x10^3$ kgm^{-3} at lower elevations, especially within the trachytic and basaltic horizons.

A Bouguer density of $2.45x10^3$ kgm^{-3} has been chosen as a compromise average density based on the results from the different analyses and the geological knowledge of the area.

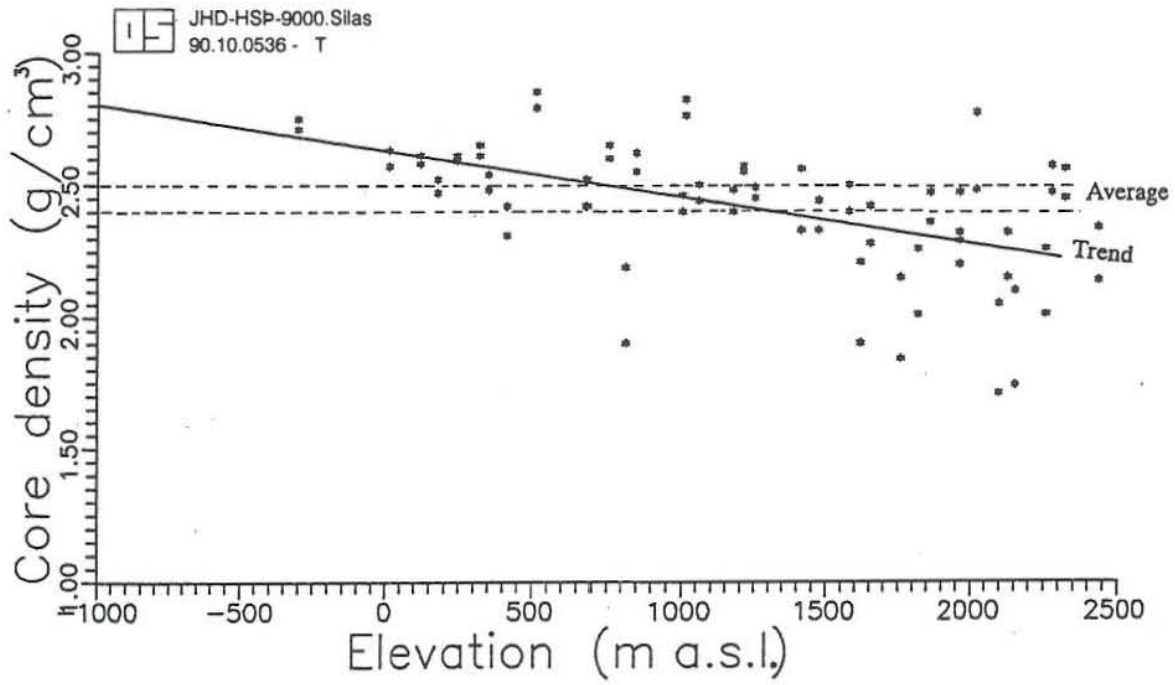

FIGURE 7: Core density vs elevation plot

5. DATA INTERPRETATION

5.1 The Bouguer anomaly map

A Bouguer anomaly map (Figure 8) was made at a scale of 1:50,000 for a Bouguer density of 2.45×10^{3} kgm^{-3} with a contour interval of 20 g.u. (gravity units). Contours were made by using a 32 X 32 gridded data with each grid unit representing 1 km. The gridding had been done by interpolation from an irregular pattern of observation stations which were made on lines along motorable tracks and consisted of closely spaced stations (200 m) around wide loops.

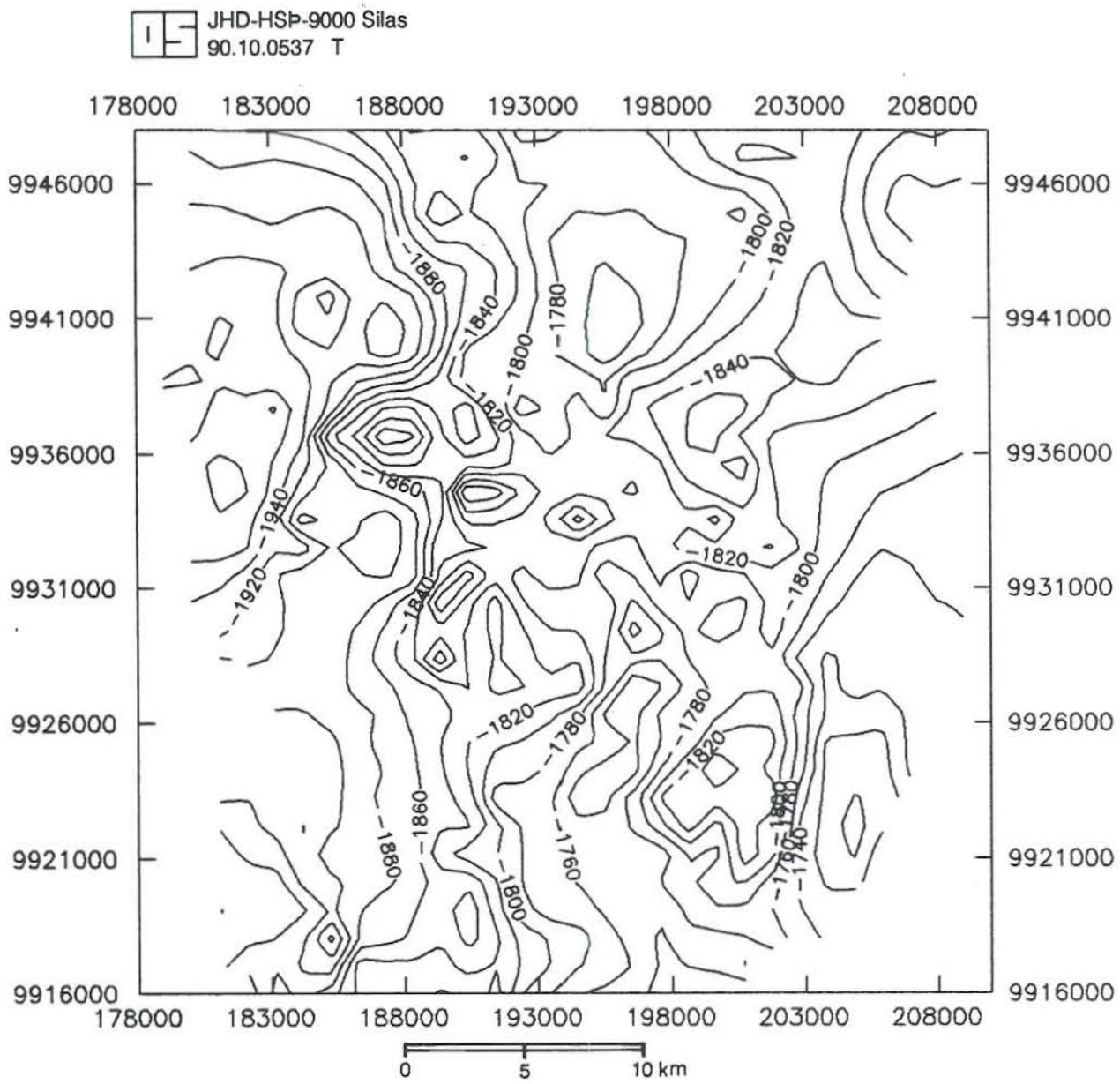

FIGURE 8: Eburru Bouguer gravity map

The anomaly varies over the area from a high positive in the east decreasing towards the western margin of the Rift valley (towards the Mau escarpment). However, the gravity increases regionally to the east beyond the survey area, presumably because of the rift axial high that stretches north-south over lake Naivasha from Olkaria. This high is well defined in the Bouguer gravity map of Kenya.

The general features of the Eburru Bouguer gravity map are:

(i) A north-south positive anomaly lying within the central region and forming an axial high (Eburru axial high) from Ndabibi in the south to the Badlands area in the north. This high anomaly shows some disturbance in the central area, dividing it into the Eburru and the Badlands highs.

(ii) A negative anomaly to the west which might extend beyond the western boundary of the surveyed area.

(iii) A north-south negative anomaly on the eastern side between the Eburru axial high and the central rift axial high.

(iv) A high on the eastern margin of the surveyed area which might be due to the rift axial high and is, therefore, a regional feature.

5.2 Regional-residual anomaly separation

The usual objective of anomaly separation is to make a map with geologically related anomalies of interest appearing as the main distinct map features. This involves the removal of a smooth regional field, and decomposition of the local residual field effects into individual anomalies by visual and numerical application of analytical techniques to an array of values on regular grids.

It is very important to note that the anomaly separation and enhancement in this study involves anomalies which have already been recognised in the original Bouguer anomaly map, and this treatment is only meant to give a clear picture of each individual anomaly.

After all corrections have been made on the data and a Bouguer anomaly map produced, the next problem is the separation of the large wavelength regional anomaly from the small residual anomaly in which we are interested.

Derivative method. The second derivatives for a given gravity field have sharper patterns than the original field and can give better separation of features relatively close together. They have an effect of removing a regional because they are related to the curvature of a gravity surface which is expected to be very small for a smooth regional surface.

In the present study the application of the second derivative resulted in a map with highly amplified high frequencies and anomalies which could not be reasonably explained. It is thought that the grid dimension used and the original station spacings had an effect on the derivative operation because large grid spacings represent only the larger features. Elements of the data which cannot be represented contribute to the noise by an aliasing process. Since the original data was not evenly spaced and noisy due to shallow intrusives, applying the second derivative amplifies the noise and creates false anomalies.

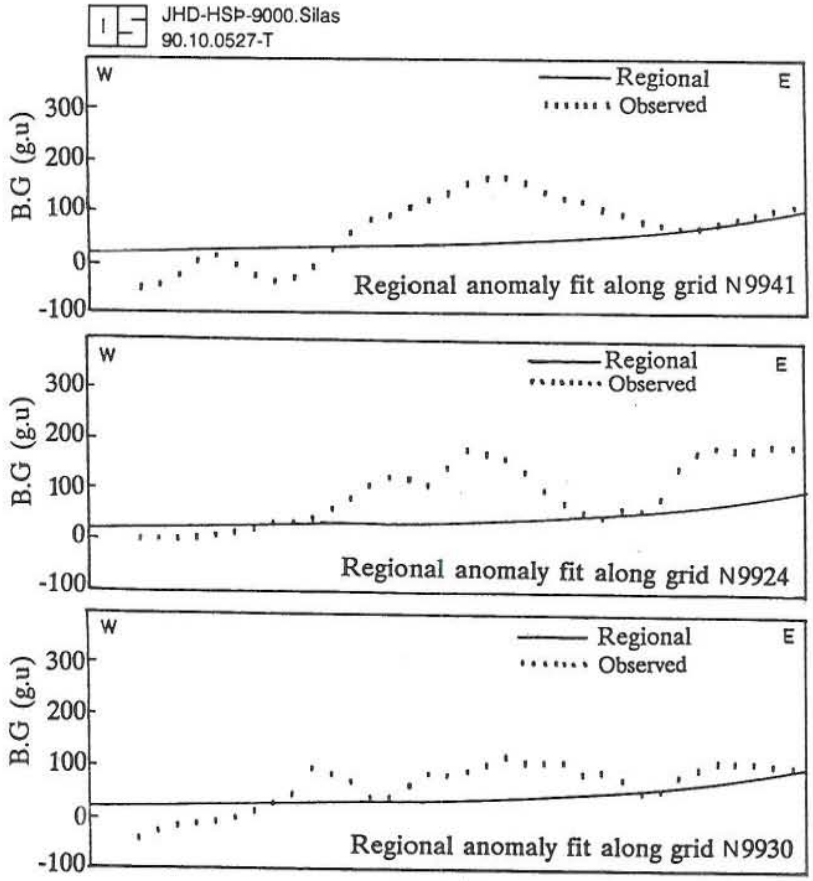

FIGURE 9: Smoothed regional E-W profiles along grid trending east; 9930000N, 9941000N and 9924000N

Smoothing method. A number of profiles were made across the Bouguer anomaly map in the direction of the regional trend and smoothing applied. A visual observation of the profiles (Figure 9) shows that the area has an east-west regional gradient of about 6 g.u. km^{-1}. Although the profiles show a reasonable trend, smoothing may not be the best method since the known regional trend is strong and not uni-directional. Due to this, the residual anomalies can easily be missed by visual methods. Also, some large anomalies that cover much of the surveyed area may be hard to discern.

Trend surface analysis. Mathematical analysis was done by using a least square statistical trend analysis decomposition program to calculate a range of polynomial surfaces which fit the input data. The degree of fit of these surfaces was statistically analyzed and outputted. Using this output information it was found that a second order polynomial surface was appropriate. The polynomial least square data fitting method was picked because it does not contain any bias, hence the trends' output are always average.

The analyzed trend was removed by using another program called LUTREND which outputted the removed regional trend (Figure 10) and the residual data (residual gravity) as separate files which were later used to make regional and residual anomaly maps (Figures 11 and 12). The second order trend surface has been found to be close to the smoothed regional gradient profiles.

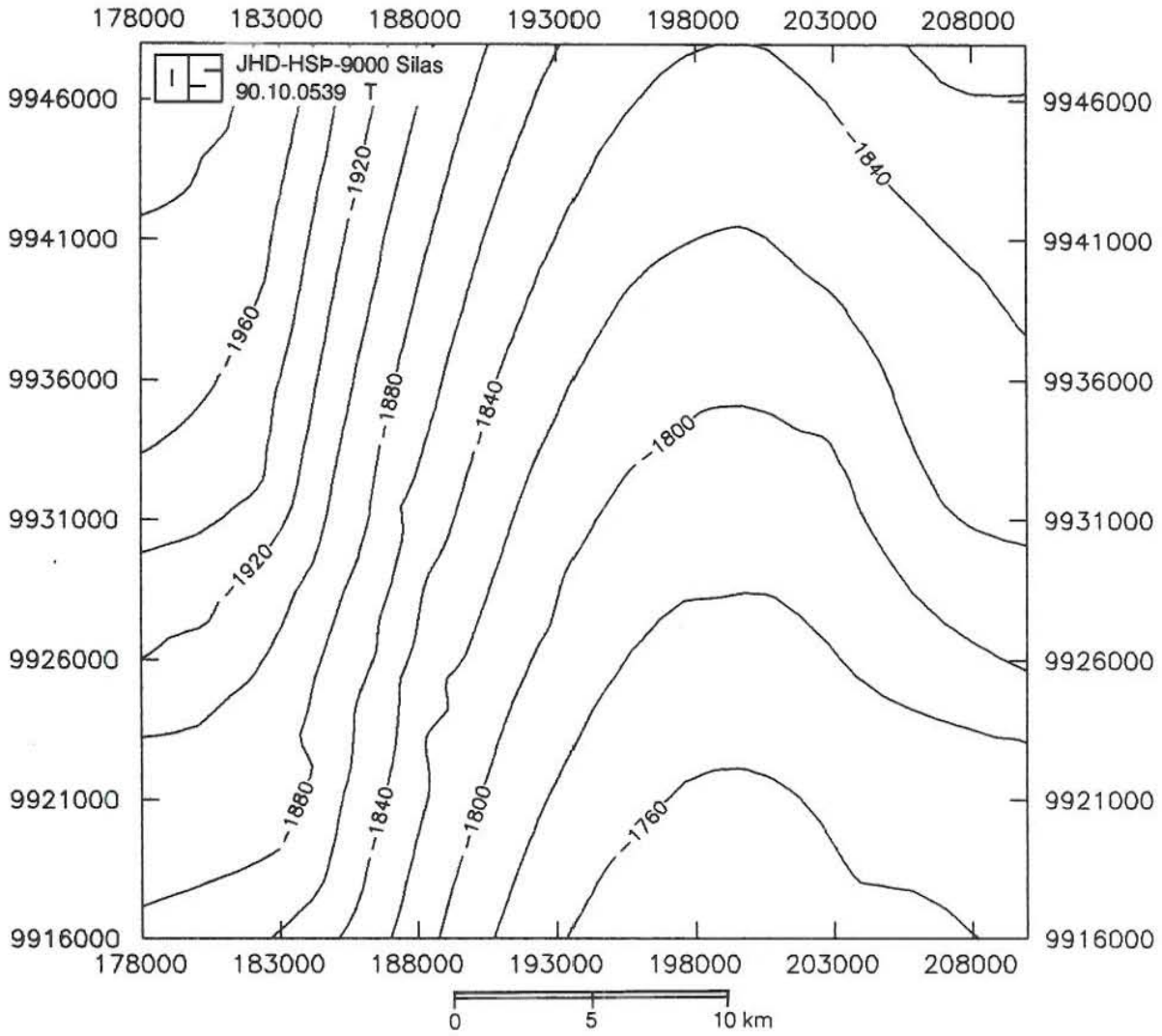

FIGURE 10: 2nd order polynomial regional gravity map

The residual gravity (Figure 11) map shows that the gravity data of the area is rather noisy due to near surface inhomogeneities. This is dominant around the Eburru crater system shown on the 3D residual gravity diagram.

The general features of the residual gravity map after removal of the regional features are:

(i) A north-south axial high in the central region which tends to die out towards the south. The structure is more pronounced in the north but is masked by noise in the central region.

(ii) An unclearly defined NE-SW anomaly of a larger wavelength with three minima in the central-east (Waterloo), central-south (Ndabibi) and southeast (Loldia). The three appear to be anomalies of the same feature disturbed by the north-south central high and other intrusive noises.

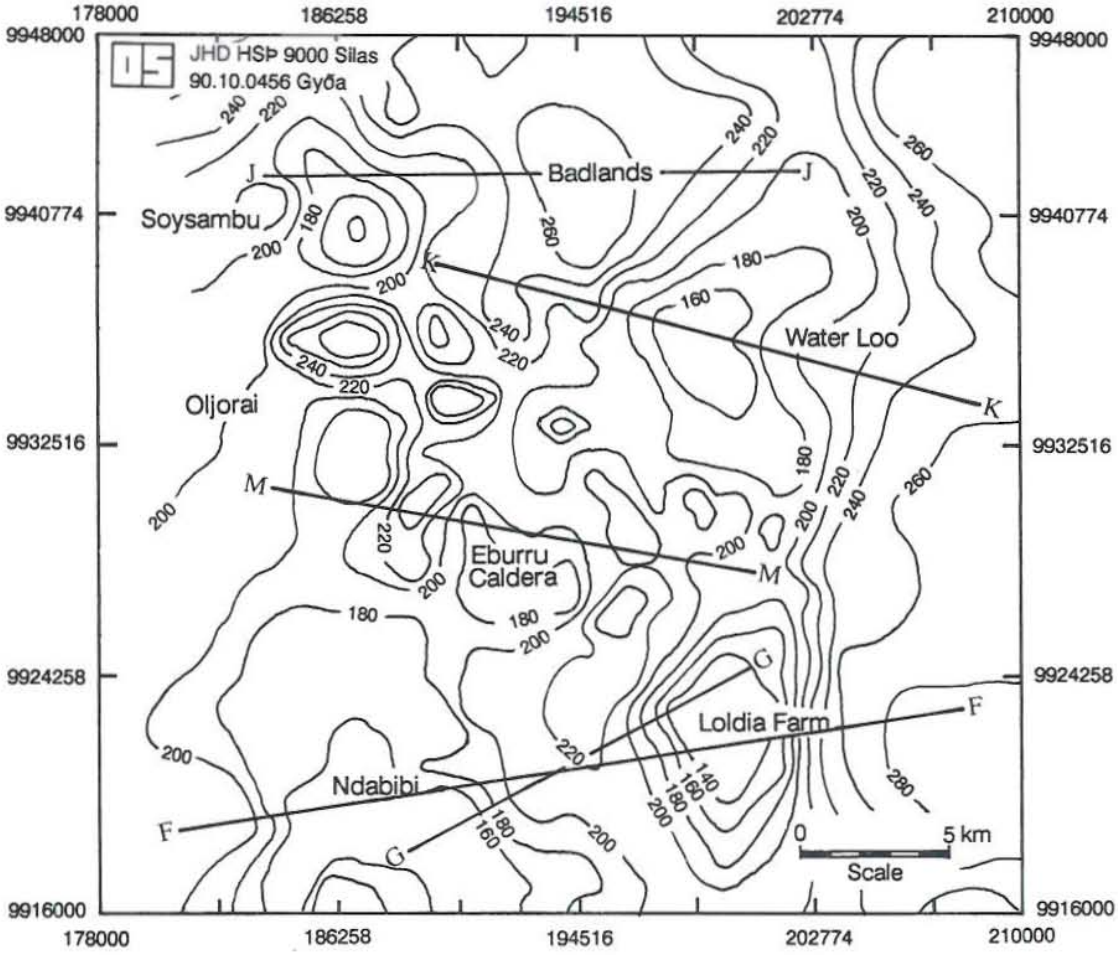

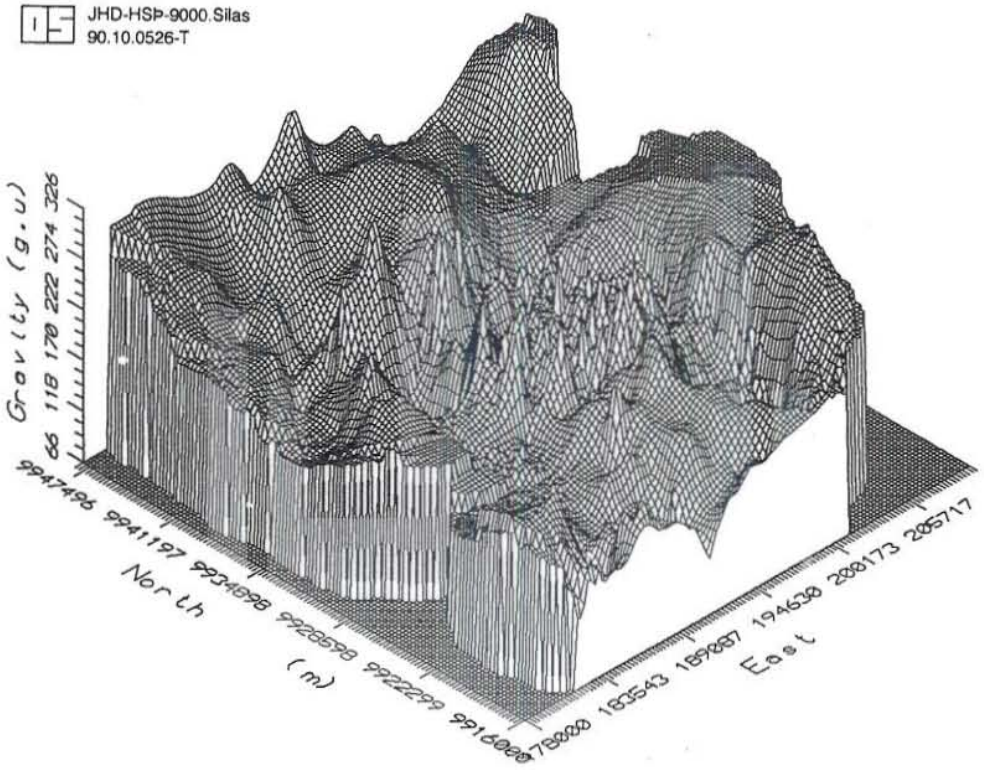

FIGURE 11: Eburru residual Bouguer gravity map and 3D diagram

(iii) A central area of small highs that may be associated with centres of intrusion and a near circular low anomaly centred on the Eburru crater system (Figure 12).

(iv) A NW-SE narrow trend of high frequency gravity lows on the northern side and associated high frequency highs on the southern side. This trend forms a narrow band which is broad to the west but diminishes to the east.

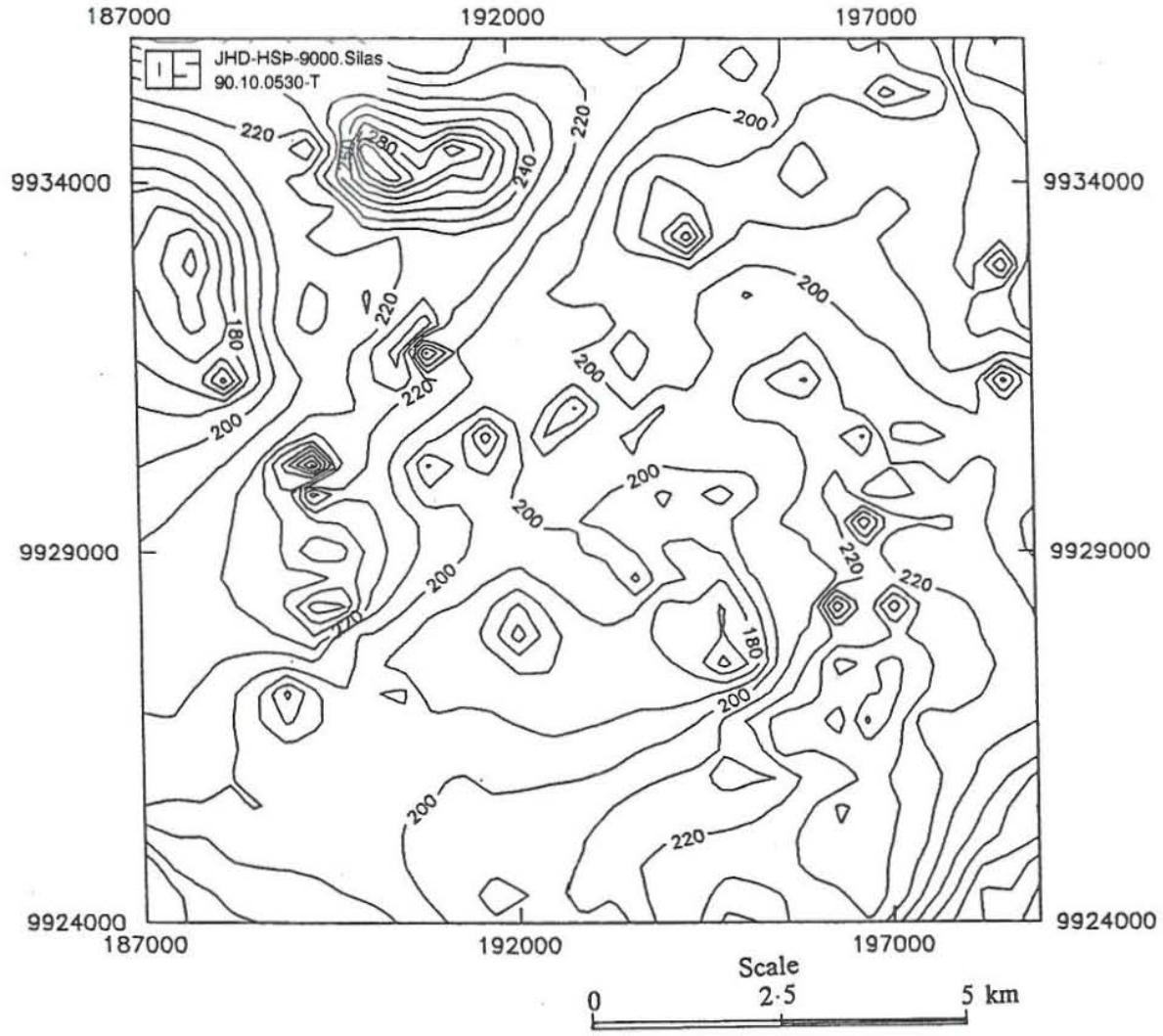

FIGURE 12: Eburru central residual Bouguer gravity map

The disappearance of the major gravity low on the western side of the area after detrending of the data agrees with the known geology of the western rift floor flanks being covered by piles of tuffs and pyroclastics that tend to suppress the gravity values on the western side. The existence of this low density material has also been inferred from seismic P-wave delay time analysis which has been carried out in the area.

5.3 Anomaly enhancement

Anomaly enhancement of residual gravity is an important method of separating anomalies of interest whose signatures merge anomalies masked by noise from shallow bodies, and is an aid to geological interpretation of buried major structural trends. The anomaly map shows features which have different periodic and directional properties. This calls for analysis of these features in the frequency domain (Thorarinsson et al., 1988; Thorarinsson and Magnusson, 1989).

The amplitude spectrum. Although personal judgement is important in choosing parameters basic to any automated system, the fundamental purpose of geophysical science is to reduce personal prejudices as far as is practical through systematic application of the rules of logic. By this, the best parameters can be chosen for analysis. Before any frequency domain operators are applied to the data, the amplitude spectrum is analyzed (Figure 13). In order to produce a spectrum without ringing, one must reduce the sharpness of the window edges. This was done by multiplying the gridded data with some function which causes the data to go down to zero at the edges. To do this, a circularly symmetric Hamming window was applied after removal of a planar trend. This window, also known as "cosine", spans the entire grid from edge to edge; the equation for its shape is given as: Amplitude = 0.5 - 0.5 ($2\pi t/T$) where, t = Distance from the edge, T = Distance across the grid and t/T goes from 0 to 1 across the grid.

It can be seen that a major linear feature dominates in a N-S direction although at somewhat higher frequencies. At lower frequencies, another feature appears in the NE-SW direction.

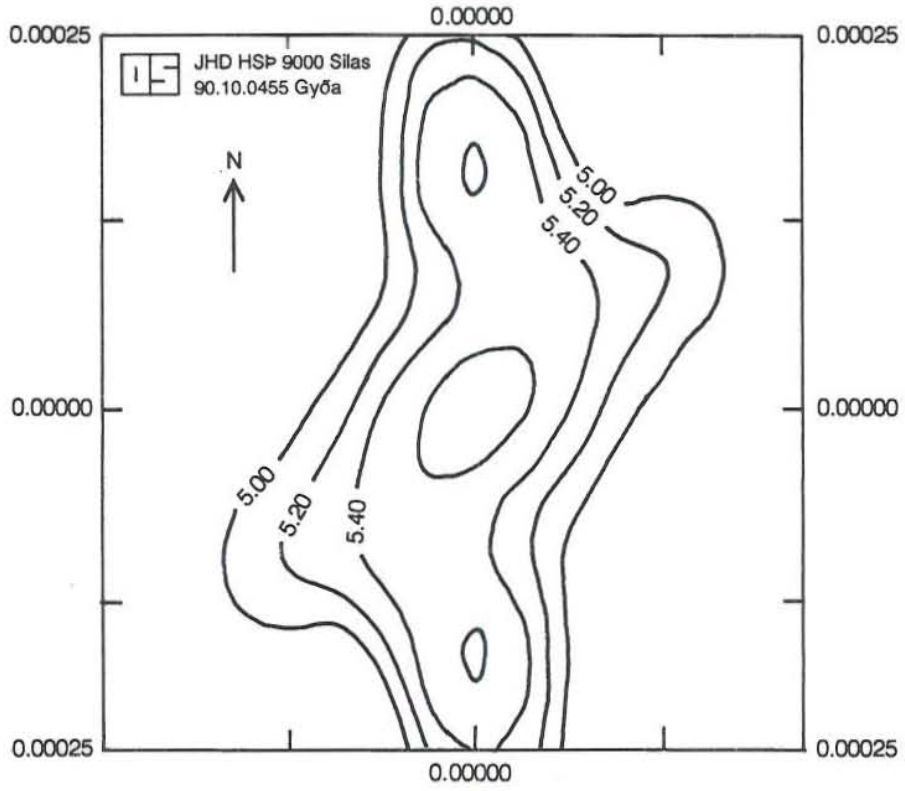

FIGURE 13: Residual gravity amplitude spectrum

The N-S structural trend is not surprising in view of the N-S rift fault trend and the surface N-S fissure swarms. The high frequency positive anomaly associated with this trend suggests that the anomaly might be due to intrusives along the fissure swarms coming close to the surface. The presence of the Badlands basalts in the north within the trend attests to this.

The NE-SW anomaly is of low frequency and may be assumed to result from a large anomaly at greater depth. This anomaly does not have near surface manifestation and is probably a tectonically extinct feature which has been covered through time.

One advantage of this essentially linear two trend spectrum is that the structures can be very easily modelled as 2D bodies. From the amplitude spectrum, the best frequencies and directional parameters to be applied during filter analysis are chosen.

Frequency filtering. During frequency analysis, different parameters within the chosen amplitude spectral range are applied. It is found that a low-pass Butterworth filter of second order with a radius of 4-6 grid units gives good maps with all the structures of interest coming up clearly. The use of a low-pass filter was also found to have less aliasing effect when tested on unwindowed data. First a 2nd order low pass Butterworth filter with cut-off at six grid units was applied to the original Bouguer gravity map after removing a planar trend (Figure 14).

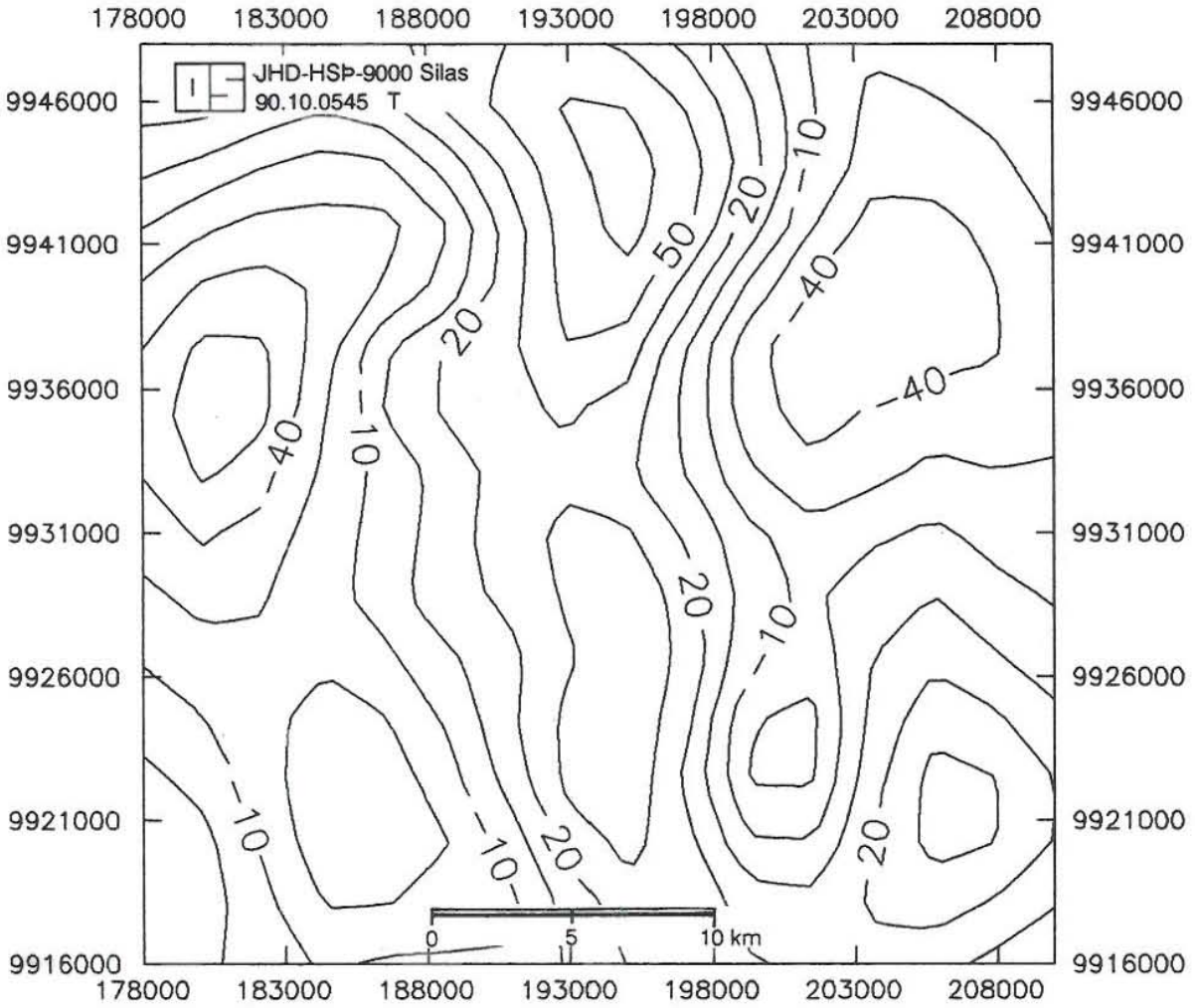

FIGURE 14: Frequency filtered Bouguer gravity map

This map shows a strong north-south anomaly trend with the central high coming out prominently. There is also a strong Bouguer increase from the west to the east due to the regional anomaly. The strong regional trend and the north-south gravity anomaly tends to mask the NE-SW gravity low trend. It may be concluded here that the regional trend tends to mask structures perpendicular to its gradient and enhances those parallel to it.

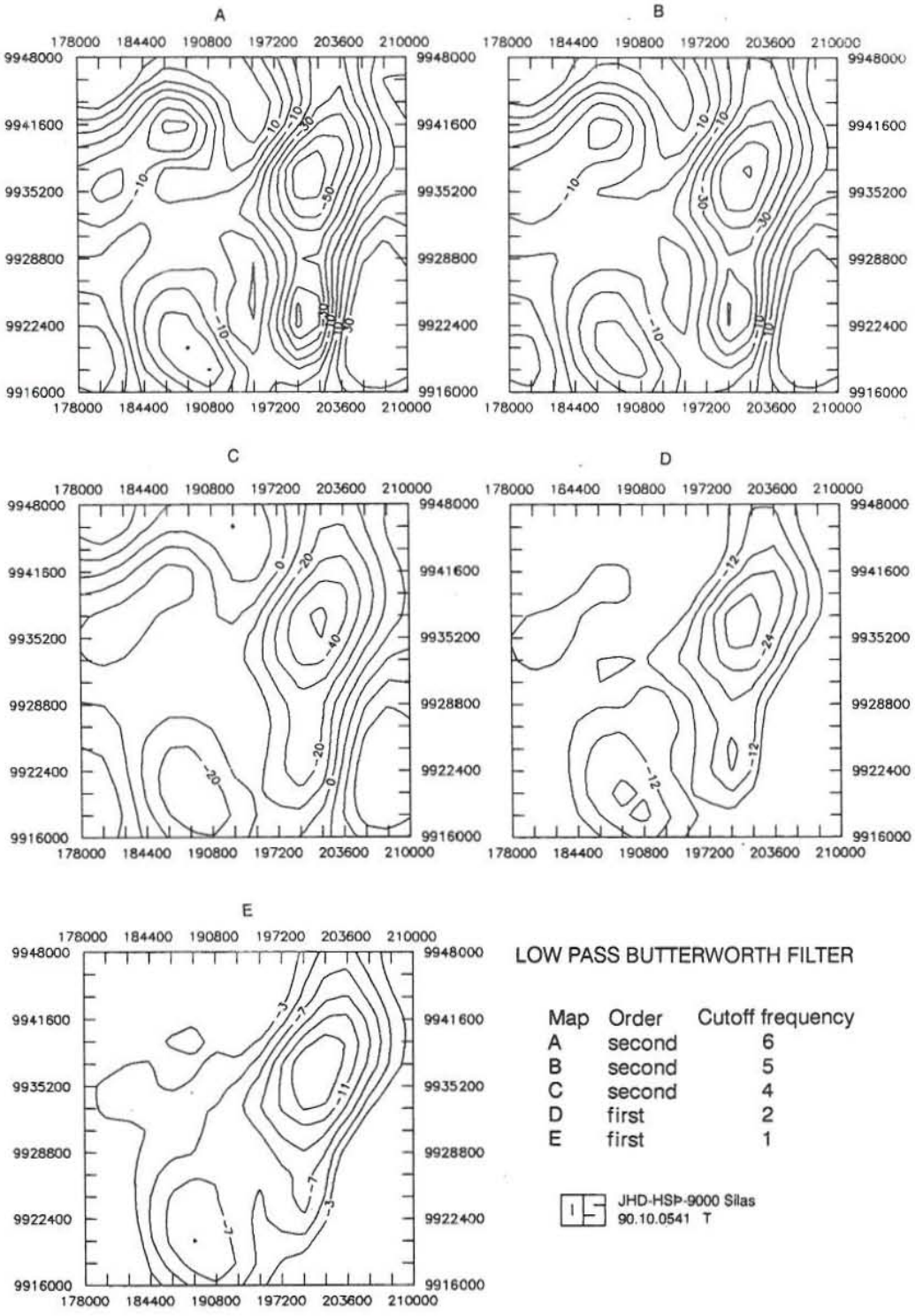

FIGURE 15: Frequency filtered residual Bouguer gravity maps

When the same parameters were applied to the residual gravity grid, the area was noticed to have two major and two minor features (Figure 15). A major NE-SW gravity low anomaly broadens to the south and is cut by a narrow north-south high anomaly that is sharply discontinued in the central part of the study area only to appear in the north as a broader feature. To the southeast is a positive anomaly which may be associated with the lake Naivasha high. A small low to the northwest with a NE-SW trend is also apparent.

When the filter parameters were changed to pass only anomalies with very low frequencies, the NE-SW structure comes out very clearly as the major deep-seated body in the area. By using the frequency filters combined with a directional fan pass filter, anomaly separation in the two main directions was made (Figure 16).

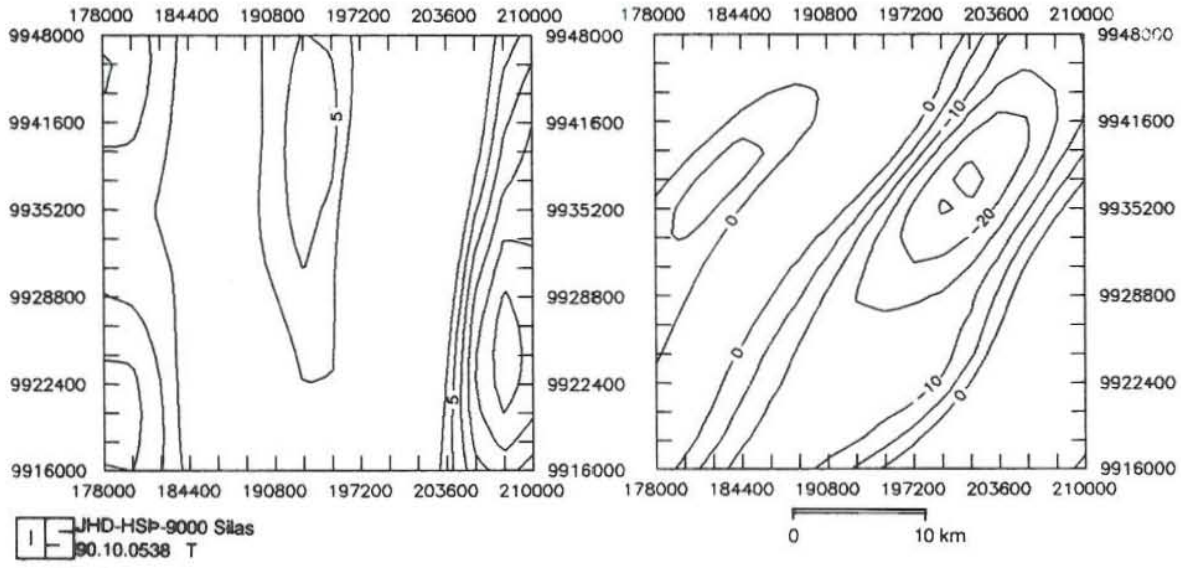

FIGURE 16: Frequency and directional filtered residual Bouguer gravity maps

Upward continuation to different elevations was also applied and the results were found to be not very different from the filtered results (Figure 17).

Downward continuation was attempted but was found to require some curtailment of the high frequency amplification. Since the area has numerous intrusives at varying depths, it was difficult to determine the optimum continuation depth, as the field continued to oscillate with the varying depths to the tops of these intrusives.

5.4 Model computations

The density values used in modelling are estimated from the Nafe-Drake P-wave velocity vs density relationship given by Grant and West (1965) and assisted by sample measurements from the Eburru wells.

The seismic P-wave velocities were obtained from the work done by KRISP (1985). The typical density value of 2.67×10^{3} kgm^{-3} has been assigned to the basement and deeper volcanics which have a P-wave velocity of 6.0 kms^{-1} obtained from KRISP (1985) and also suggested by

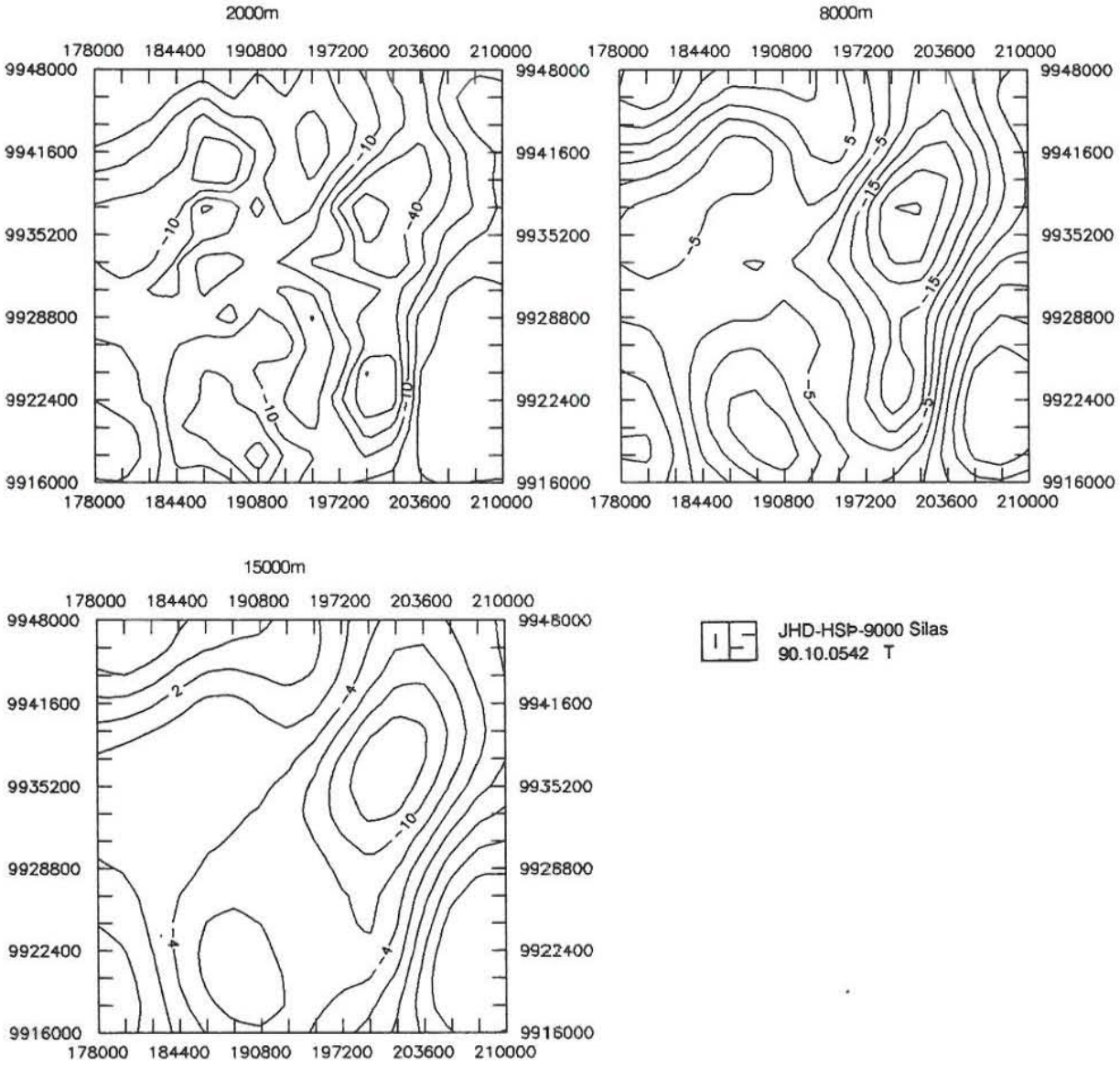

FIGURE 17: Upward continued residual Bouguer gravity maps

Fairhead (1976). The near surface volcanics with a P-wave velocity of 3.8 kms^{-1} have been assigned a density of $2.15x10^{3}$ kgm^{-3}.

The residual gravity map shows two major anomalies that are quantitatively modelled using a computer program called MAGRA (Thorarinsson, 1985): the N-S positive anomaly from the Badlands in the north to Ndabibi in the south and the NE-SW negative anomaly from the east of the Badlands to the west of Ndabibi.

5.4.1 E-W gravity profiles

For the purpose of obtaining a structural picture for the gravity data, a number of profiles in an E-W and NW-SE directions across these anomalies are modelled (for location see Figure

11). These profiles are nearly perpendicular to the two major anomaly trends and known faults. One N-S profile is modelled to define the interruption in the gravity high near Eburru station by a narrow NW-SE graben structure. The modelling assumption is that the residual anomalies are due to sources extending from near the surface downwards to below sea level. The gravity highs are interpreted as being due to the intrusion of dense magma-derived material into the country rock along fault zones. This material is assumed to be basaltic or trachytic with an average density of 2.75×10^3 kgm^{-3}, and provides a density contrast which decreases with depth as the country rock density increases.

Although the models are simplified, the actual bodies may be in the form of single bodies or numerous dykes. Thus, the anomalous zone may be half country rock material and half dykes with a wide intrusion zone, thus reducing the density contrast values.

Profile FF. This is an E-W profile located close to the southern boundary of the surveyed area. It was made to pass through the two southern gravity lows of Ndabibi and Loldia farm and the central north-south high.

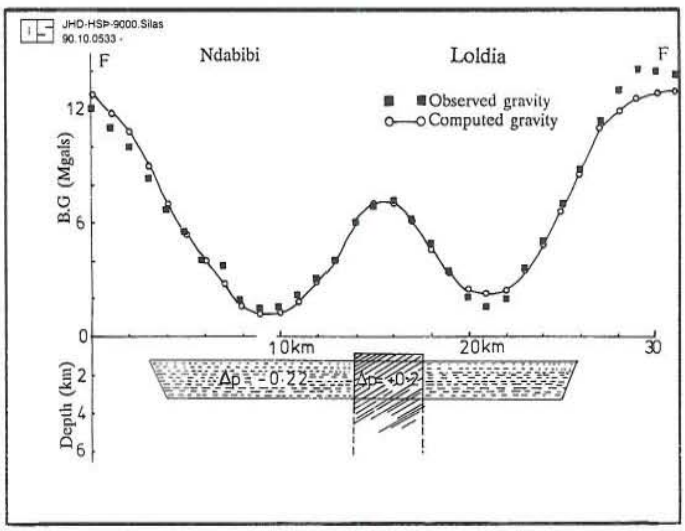

FIGURE 18: Model fit on residual Bouguer anomaly profile FF

The aim of this profile (Figure 18) is to define the depth and width of the body causing the broad NE-SW gravity low inferred from the frequency filtered data as being caused by a single large basin. It is also meant to determine the relationship between the low density basin and the body causing the N-S positive anomaly. The basin is modelled as a -0.22×10^3 kgm^{-3} density contrast body, 3.2 km deep and 21 km across. The central high is modelled as a dyke intrusion within the basin of density contrast 0.2×10^3 kgm^{-3}, 800 m below the surface and 3.6 km across.

Profile KK. This profile (Figure 19) is located north of the Eburru massif to the east of the Badlands area across the Waterloo ridge low. It is aimed at determining the extent and depth of the gravity low basin which extends from the northeast to the south. A 6.5 km wide body of density 2.23×10^3 kgm^{-3} and a depth of 3 km to the bottom gave a good anomaly fit.

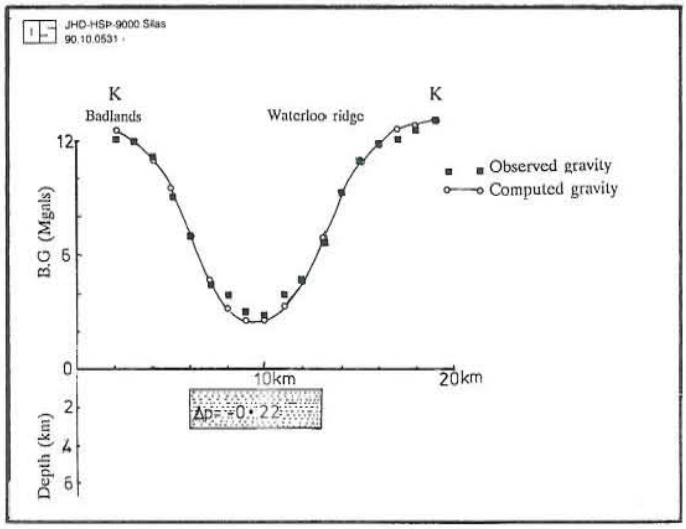

FIGURE 19: Model fit on residual Bouguer anomaly profile KK

Profile GG. This profile (Figure 20) is to the south of the Eburru massif across the N-S positive anomaly. It is made to determine the depth and thickness of the causative body without including the broad basin effects. The body is modelled to be 2.65×10^{3} kgm^{-3} dense at 500 m depth with a thickness of 3.4 km.

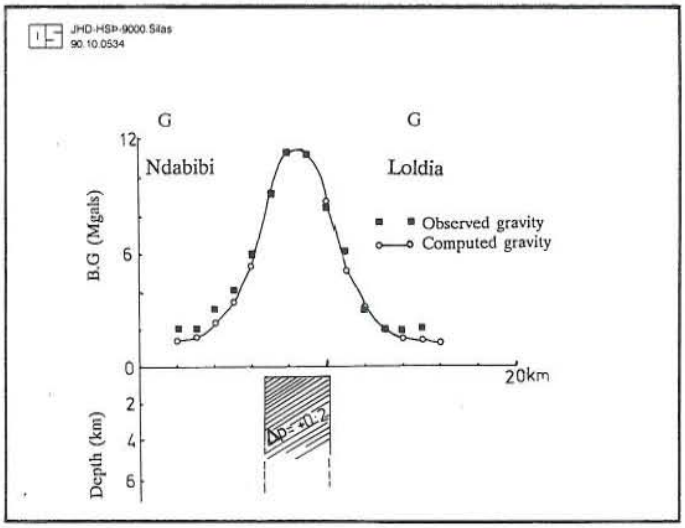

FIGURE 20: Model fit on residual Bouguer anomaly profile GG

Profile MM. This is an E-W profile located close to grid line 9930000, purposely made through the Eburru crater system and close to Eburru wells EW-01 and EW-04 from which core densities have been determined. The profile (Figure 21) shows a negative anomaly inside the Eburru crater and two positive anomalies on the sides.

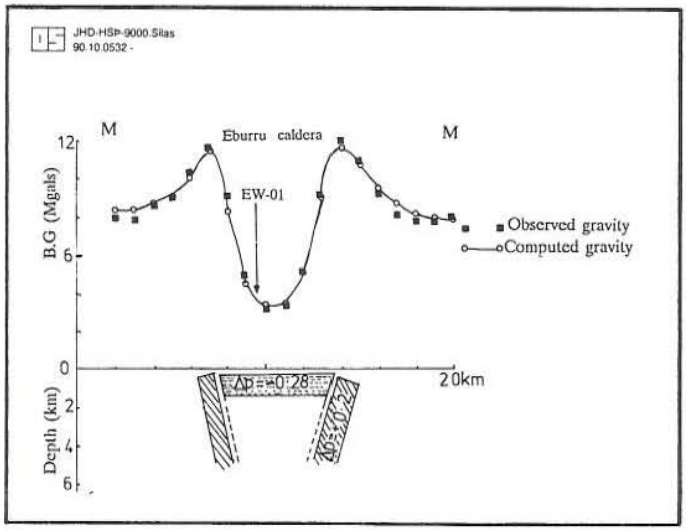

FIGURE 21: Model fit on residual Bouguer anomaly profile MM

The central area negative anomaly is modelled as a 500 m slab of low density material (2.13×10^3 kgm^{-3}) due to downfaulting then filling by pyroclastic material and the two positives as dipping, 2.65×10^3 kgm^{-3} dense, dyke-like intrusives coming to within 250 m of the surface. These intrusives have a thickness of 0.8 km on the western side and 1.4 km on the east. Both dip towards the central crater.

Profile JJ. This profile (Figure 22) is to the north of Eburru hill within the Badlands basalts area. The aim of the profile was to determine the dimensions of the body causing the high. Because the body is not two dimensional, a vertical cylinder was applied and modelled at a depth of 2 km to the top. It is 3.4 km thick with a density of 2.75×10^3 kgm^{-3}.

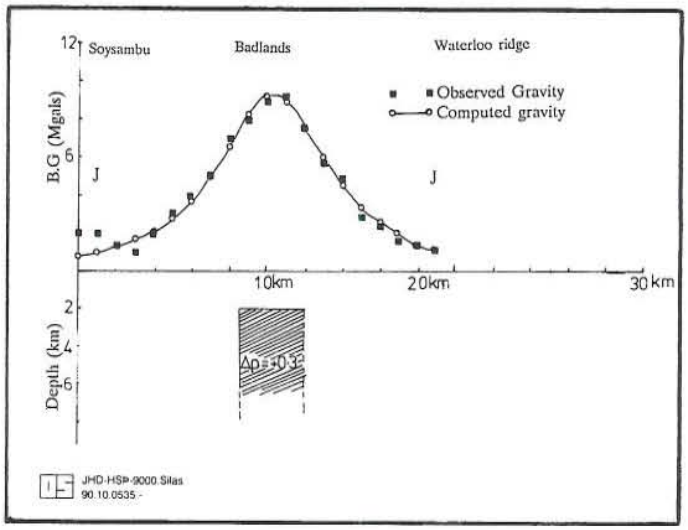

FIGURE 22: Model fit on residual Bouguer anomaly profile JJ

5.4.2 The N-S trending resistivity profile SN

This profile was made in a N-S direction along the axis of the N-S central high from Badlands in the north to Ndabibi basin in the south. The profile (Figure 23) was aimed at determining variations in the depth to the top of the axial high body, especially at points of intersection with the NE-SW trend and the narrow NW-SE graben. The profile was intended to follow a 2D modelled resistivity profile (Figure 24) to act as a control on modelling.

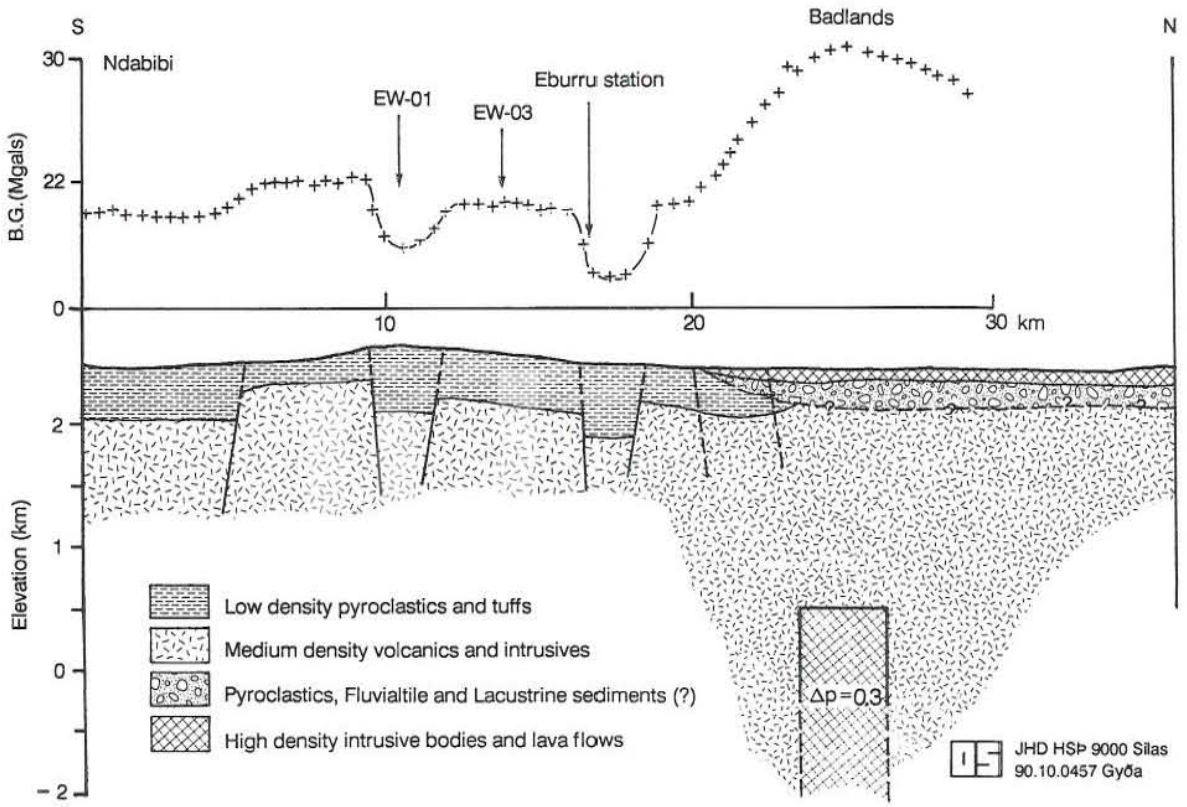

FIGURE 23: Model fit on residual Bouguer anomaly profile SN

A visual observation of the profile reveals that this N-S body is not continuous along its axis but is cut at several places into some sort of step platforms, notably the crater area with a downthrown block, the area crossed by the NE-SW trend and the NW-SE narrow graben area. To the north, the anomaly high does not appear to be caused by this block type of structure but by a deep-seated body unrelated to the faulting phenomenon.

To model this profile, it was found convenient to break it down into 5 different profiles, each with a step and two platforms. Fault modelling with a horizontal slab was applied to each of the profiles and the throw calculated. Since this profile crossed some of the already modelled features and two of the drilled wells (one well in the crater and the other on the next block), determination of the starting parameters for modelling the faults was rather easy.

To the north the gravity high is modelled as a combined effect of a fault and a dyke structure in the shape of a vertical cylinder at a depth of 2 km. After each individual fault and body had been determined, they were all stuck together to make a sketch section.

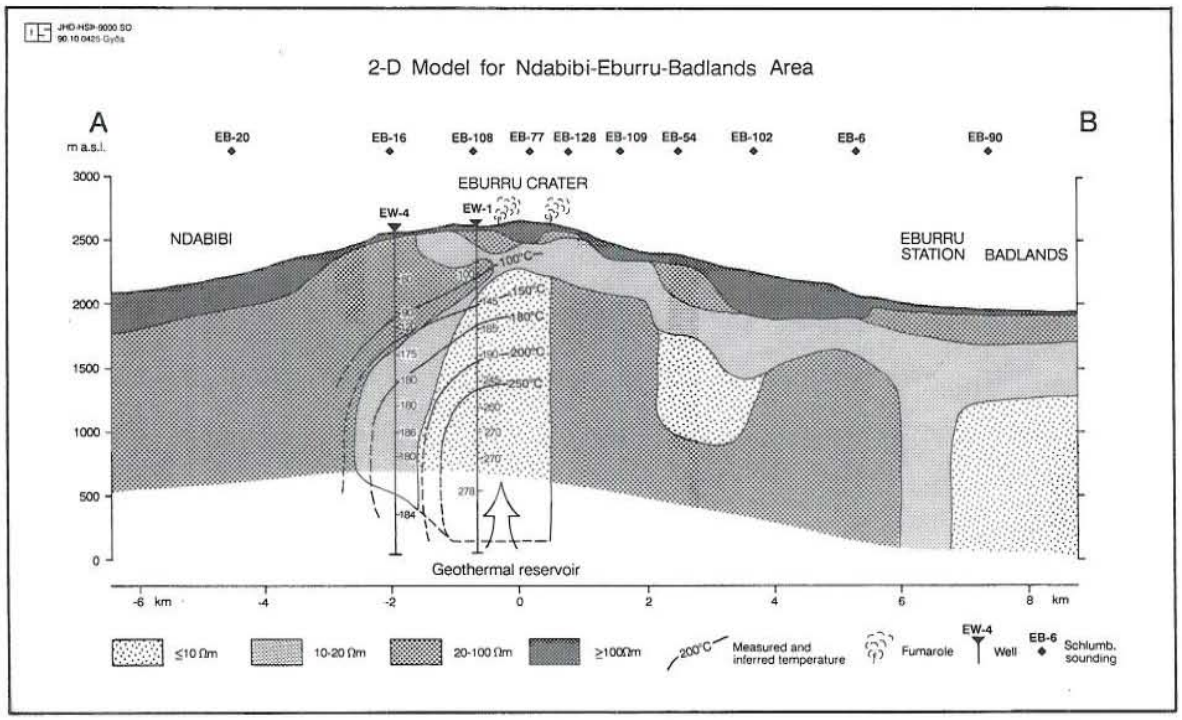

FIGURE 24: Resistivity section along gravity profile SN (Onacha, 1990)

5.5 Discussion of models

The models used in this study are simple with regular geometrical shapes thus making modelling easier with less accurate results. This means that the dimensions determined during modelling are just approximations.

For the N-S gravity high, 2D bodies were used as a means of estimating the depth to the centre using the Bott-Smith method. Although this anomaly has dimensions in the N-S direction greatly exceeding the E-W direction, the body is not essentially linear with a varying wavelength and amplitude. An unconstrained two dimensional model cannot give a good estimate. The positive anomaly to the north is closer to 3D than 2D; therefore, the values obtained by manual calculation using a vertical cylinder model are reasonable.

Although the limitations discussed reduce the quality of interpreted results, they are nevertheless reliable as long as the estimations obtained are treated as such. Where fault throws have been modelled, the values obtained are in close agreement with well core data and 2D resistivity model (Figure 24).

6. DISCUSSION

The filtered residual gravity map and modelled profiles indicate that the NE-SW low gravity anomaly body is a basin of essentially constant density contrast which widens towards the south and has been dissected by a high density N-S body, thus dividing the basin into two parts, the Loldia farm and the southwest (Ndabibi). The Loldia farm and the northeast lows are divided by a NW-SE trend of gravity lows and highs. At Loldia the association of a gravity low with a positive magnetic anomaly (Figure 25) and high resistivity suggests that the basin here is deposited by low density pyroclastic material with very low magnetic susceptibility.

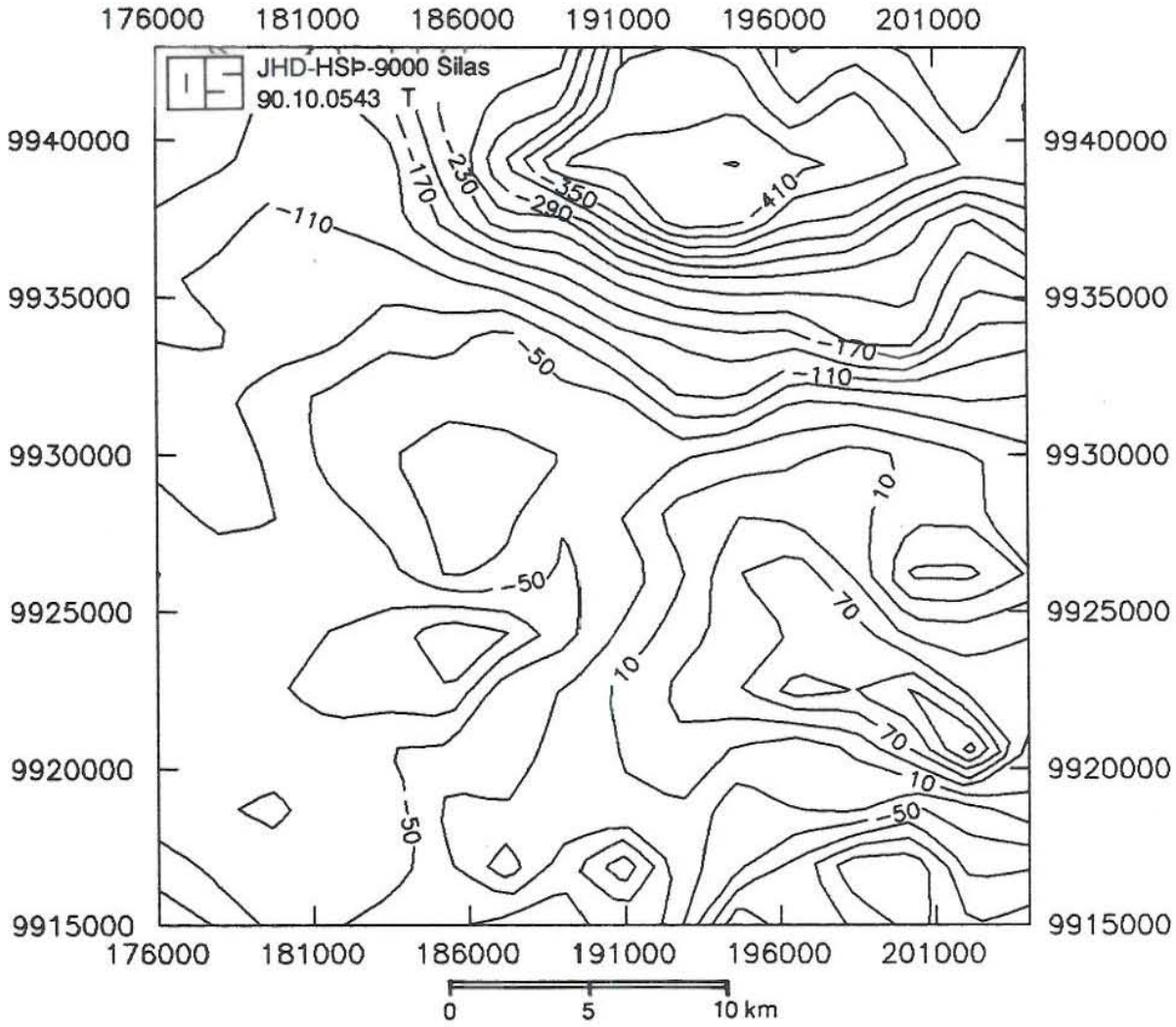

FIGURE 25: Eburru magnetic anomaly map

To the southwest, an increase in the thickness of volcanics is responsible for the negative anomaly. As shown on the N-S gravity model (Figure 23), this may be caused by the NE-SW structural trend, the N-S graben structure through the Eburru massif and a NW-SE fault structure with a throw to the south between Eburru and Ndabibi. Hamilton et al. (1973) showed that the seismic receiver stations located toward the southwestern part of the study area were associated with large travel time delays relative to the stations to the east and the north. This indicates that there is an increase in the thickness of low density material in the region. The extension of this southwest low through Eburru to the northeast area is of interest since there

is not much collaborative evidence from other geophysical data to suggest the presence of a basin structure. The amplitude of this structure is maximal within an area which is thought to have been part of a large Lake basin that extended from Lake Nakuru in the north to Olkaria in the south. This area is also part of a broad resistivity low that is thought to be caused by lake sediments. If this line of thought is true, then the gravity low may be due to a deeper part of the basin filled by sediments. The other possibility is that since the area lies between the Badlands basalts gravity high and the known Rift valley regional high, if the regional correction is not done properly then it can create a negative anomaly, although the known amplitude and wavelength of both the regional and the Badlands highs cannot create an anomaly of such amplitude. The Eburru structural map (Figure 26) shows that there are faults in the northeast area whose overall throws form a basin structure. The map also shows a number of not well developed NE-SW faults whose overall effect is a NE-SW graben structure.

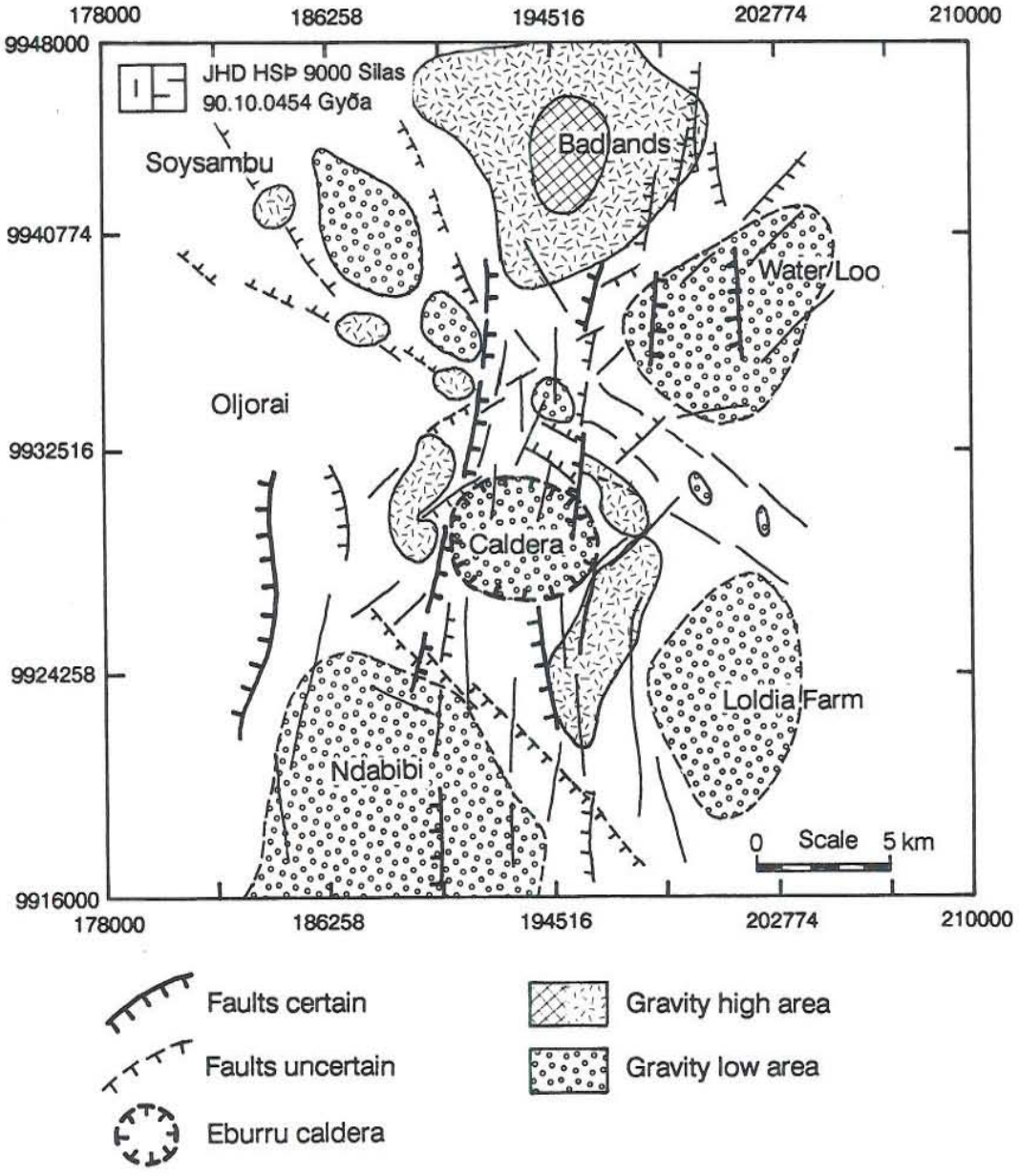

FIGURE 26: Eburru Bouguer gravity structural map

Considering the Rift valley trend at Eburru (Figure 27), if there is an opening up as is believed, then the NE-SW trend will be a significant zone of shearing and transform motion. This continuous zone of gravity low defines a major structural trend and may delineate a deeply buried fault zone.

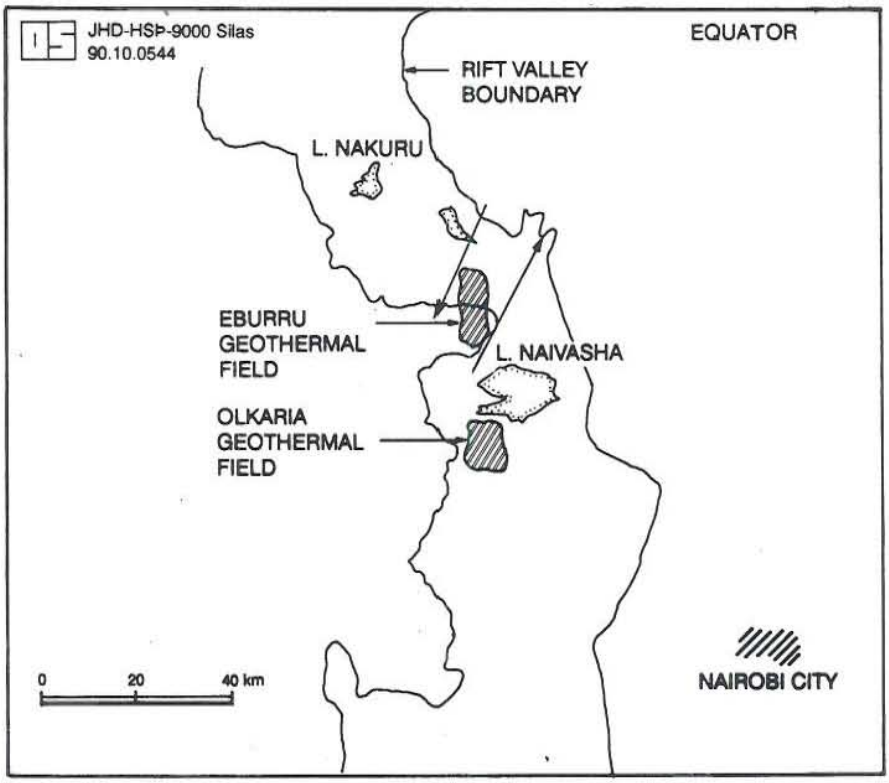

FIGURE 27: Rift valley trend at Eburru

The Badlands and Eburru highs appear to have been intruded along the same line of weakness which extends from the south northwards. However, the two appear to have been intruded during different episodes, with the Badlands being at a later phase. The Eburru body is narrow and elongated N-S while the Badlands one is cone shaped. The magnetic anomalies support this as the Badlands is normally magnetized and the one in the south is reversed.

As seen on the modelled profiles, there is not a single N-S body but rather bodies following the N-S rift trend due to intrusion along faults which occur in this direction.

On the sketch gravity map of the central Eburru area (Figure 28), the N-S gravity high appears as two tongues, one from the north and the other from the south. Close to the Eburru caldera the highs thin out and take orientations controlled by the NE-SW trend and the ringed caldera. The split of this high into two, with the southern part pulled towards the northeast and the northern part towards the southwest, is in good agreement with their expected motion if the rift is opening up. One well, drilled within this gravity high to a depth of 2700 m, encountered at 1200 m a granitic rock with low temperature and permeability. This means that the heat source in Eburru is not related to this main intrusive body but rather to minor intrusives within the caldera of a later phase, which are easily treated as noise in gravity modelling.

A series of N-S faults form a graben structure from the south of Eburru to Badlands in the

north. At Eburru, the intersection of this graben structure and the NE-SW gravity low trend is the Eburru caldera which could have been formed as a result of a collapse in the central region, then some intrusive occurrences at the N-S and NE-SW fault junctions, thus creating the local gravity highs and lows. The amount of low density material infill in the caldera is 500 m maximum which is very small. The N-S faults forming the graben structure are expected to continue for a short distance beneath the Badlands basalts.

A narrow NW-SE graben structure divides the study area into the Eburru massif and the Badlands to the north. This graben widens to the northwest and the gravity highs appear to be due to intrusives coming up at junctions of this structure and deep N-S faults. This structure is also defined by a resistivity discontinuity, and is thought to have been the source of the basalts flow, later covered by pyroclastics. The gravity lows are associated with low resistivities in this graben.

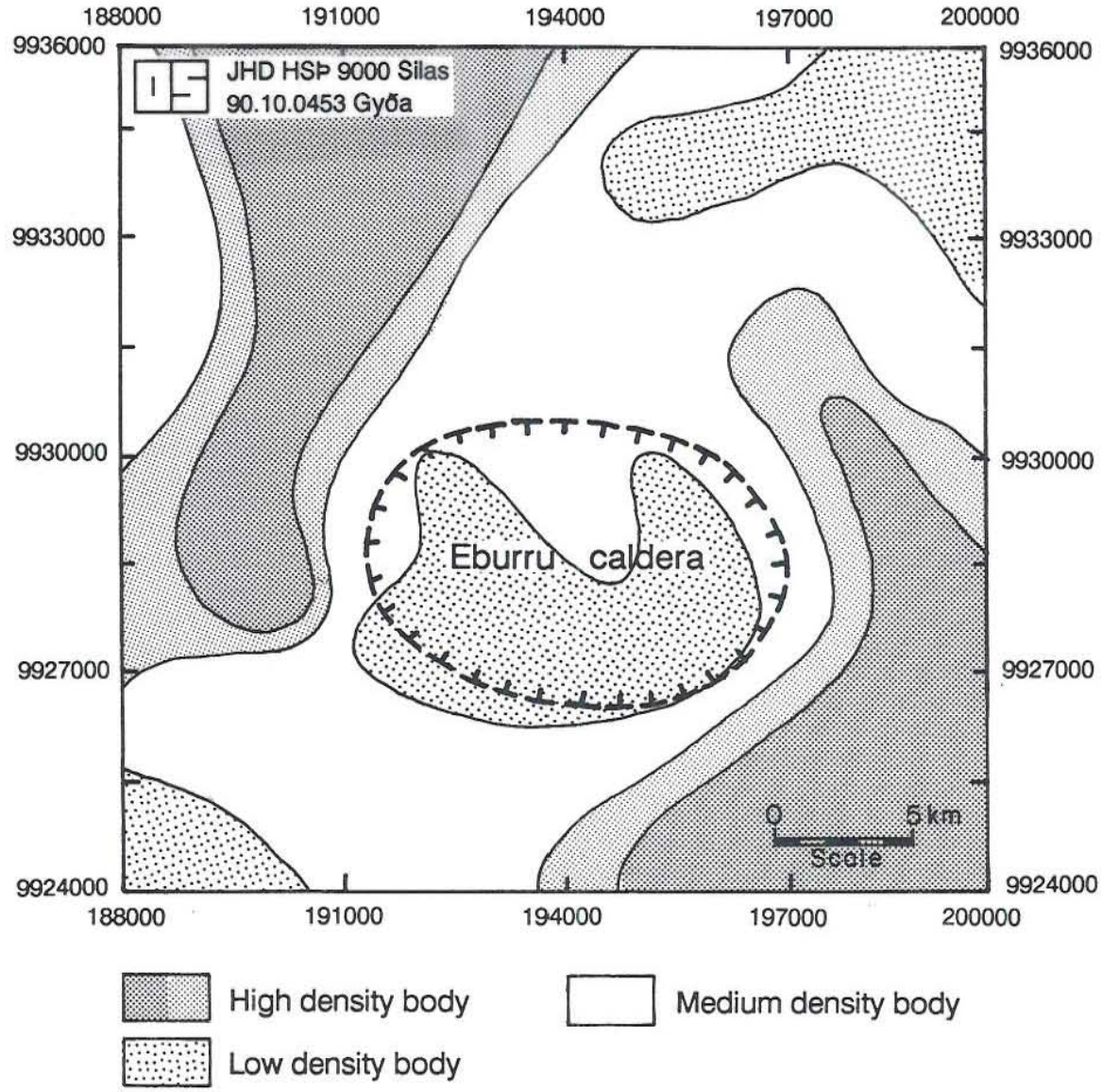

FIGURE 28: Sketch map of central Eburru Bouguer gravity

7. CONCLUSIONS

(i) There is no direct connection between the main gravity highs and a heat source.

(ii) Intrusion of high density bodies occurs along fault zones.

(iii) The Eburru caldera is covered by low density pyroclastics of a thickness less than 500 m and intruded by narrow volcanic bodies which may be related to a heat source.

(iv) There exists an NW-SE buried graben structure that divides the Eburru massif from the Badlands area. This discontinuity with low density material is important as low resistivities have been found in it.

(v) There occurs a major low frequency NE-SW structure which may be related to the rift structure with the Eburru caldera occurring at its intersection with the N-S graben structure.

(vi) Several intrusions exist at the intersections of the NW-SE structure and the N-S fault zone west of the Eburru volcano.

8. RECOMMENDATIONS

(i) For an accurate determination of the regional anomaly values in the Eburru and Olkaria geothermal area, an east-west regional gravity survey across the Rift valley and passing through the two areas is necessary.

(ii) The NE-SW gravity low structure passing through the area needs more study. The understanding of it could explain the occurrence of the Eburru geothermal system.

(iii) To test the gravity interpretation, a well should be drilled at the intersection of the NE-SW structure, the NW-SE graben, and the N-S graben on a resistivity and gravity low. This well will also serve as a control for future work towards the north.

(iv) Because the available magnetic data has been filtered, it was found difficult to use it as the filter parameters used were not known. An attempt should be made to get the original data and model it over the gravity anomalies.

ACKNOWLEDGEMENTS

I wish to acknowledge the government of Iceland and the United Nations University for providing me with financial assistance to attend this course, the Icelandic National Energy Authority (Orkustofnun) for providing the teaching staff and the Kenya Power Company for granting me sabbatical leave.

Much thanks are due to the UNU Geothermal Training Programme director Dr. Ingvar B. Fridleifsson, Mr. Ludvik S. Georgsson and Mrs. Marcia Kjartansson for their motivation and guidance throughout this study period.

Dr. Freyr Thorarinsson, who supervised this project to it's completion, receives my deepest appreciation.

To my wife Jane, daughter Belinda and son Edgar, I say thanks for their six month sacrifice during this course.

REFERENCES

Grant, E.S. and West, G.F., 1965: Interpretation theory in applied geophysics. McGraw-Hill Book Co., U.S.A., 583 pp.

Fairhead, J.D., 1976: The structure of the lithosphere beneath the Eastern Rift, East-Africa, deduced from gravity study. Tectonophysics, 30, 269-298.

Hamilton, R.M., Smith, B.E. and Knapp, F., 1973: Earthquakes in geothermal areas near Lake Naivasha and Hannington, Kenya. UNDP/EAPL Geothermal exploration project, report, 66 pp.

JICA, 1983: Pre-feasibility study report for the Rift Valley Geothermal development project. JICA., 55 pp.

KPC, 1986: Scientific review and well siting meeting. KPC report prepared by Genzel, Auckland.

KRISP, 1985: Structure of the Kenya Rift from seismic refraction. Nature, 325, no. 6101, 239-242.

Nettleton, L.L., 1976: Gravity and magnetics in oil prospecting. McGraw-Hill Book Co., U.S.A., 464 pp.

Ng'ang'a, M., 1989: Assessment of topographic and demagnetization effects of airborne magnetic anomalies in Eburru prospect, Kenya. Geothermal Institute, Auckland., report 89.16, 47 pp.

Onacha, S.A., 1990: Application of Schlumberger sounding at Eburru, Kenya and TEM and MT methods at Bakki, S-Iceland. UNU G.T.P., Iceland, report 11, 52 pp.

Swain, C.J. and Khan, M.A., 1977: Kenya: A catalogue of gravity measurements in Kenya. Leicester University, Geological department, report, 30 pp.

Thomson, A.O. and Dodson, R.G., 1963: Geology of the Naivasha area. Geol. Surv. Kenya, report 55, 80 pp.

Thorarinsson, F., 1985: MAGRA, version 1.20, two-dimensional graphically interactive modelling of gravitational and magnetic anomalies. Report and programme (unpublished), 44 pp.

Thorarinsson, F. and Magnusson, S.G., 1989: STRIKE, version 4.0, gravity and magnetic data management and processing routines. Report and programme (unpublished), 65 pp.

Thorarinsson, F. and Magnusson, S.G., 1990: Bouger density determination by fractal analysis. Geophysics, 55, 932-935.

Thorarinsson, F., Magnusson, S.G. and Björnsson, A., 1988: Directional spectral analysis and filtering of geophysical maps. Geophysics, 53, 1587-1591.